

RAM

● ROBOTICS
AND
MECHATRONICS

DESIGN AND CONTROL OF EFFICIENT AND POWERFUL ROBOT JOINTS

W. (Woong) Kim

MSC ASSIGNMENT

Committee:

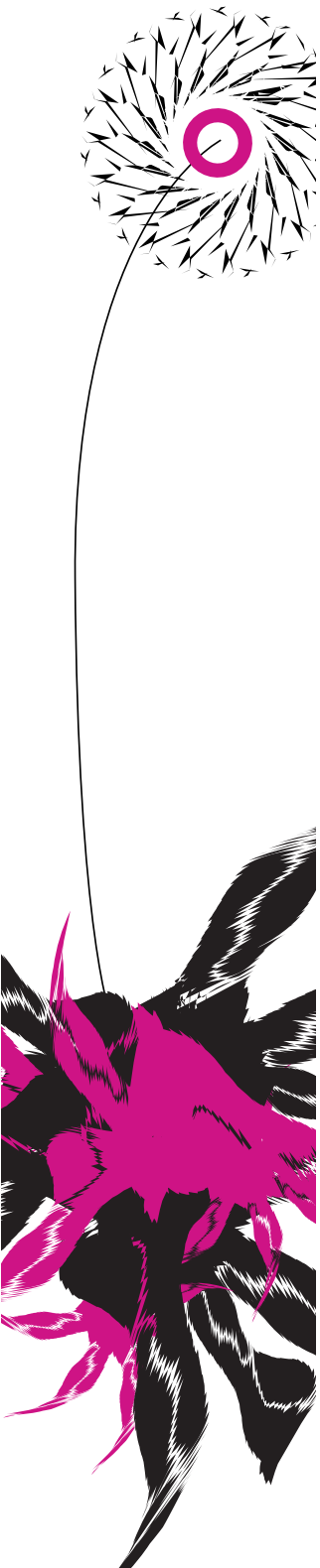
prof. dr. ir. S. Stramigioli

dr. ir. W. Roozing

dr. ir. A.Q.L. Keemink

September, 2022

045RaM2022
Robotics and Mechatronics
EEMCS
University of Twente
P.O. Box 217
7500 AE Enschede
The Netherlands



Abstract

Despite several advantages such as simplicity, controllability and backdrivability, one drawback that direct-drive actuator has is the power loss caused mainly by Joule heating. This results in poor energy efficiency and limits the maximum forces(torques) of the motors. Among all the actuator designs proposed to overcome the limitation of single direct-drive(DD) motors, two types of actuators have been widely used; quasi-direct drive(QDD) and series-elastic actuator(SEA). However, neither of them can perfectly resolve the issue due to their intrinsic disadvantages; low torque capacity or density for QDD and low control bandwidth of SEA. In the first part, this paper introduces a method of designing both types of actuators with optimally selected parameters, as well as a straightforward and effective procedure of controller design for nonlinear robot dynamics. In order to take advantage of the possible strong points as well as getting rid of the disadvantages of both two types of actuators, a novel way to combine two concepts will be introduced in the second part of this paper. Through simulations using 1-DOF and 3-DOF robot models, it is shown that a redundant actuator model having the same weight of that of DD, similar tracking performance, better energy efficiency and bigger forces(torques) can be designed.

Contents

| | |
|---|------------|
| Abstract | iii |
| 1 Introduction | 1 |
| 1.1 Problem Statement | 1 |
| 1.2 Related Works | 2 |
| 1.3 Contributions | 3 |
| 1.4 Research Questions | 4 |
| 1.5 Report Layout | 4 |
| 2 Modelling | 5 |
| 2.1 Types of Actuators | 5 |
| 2.2 Frictions | 6 |
| 2.3 Robot Dynamics : 1-DOF Robot Arm | 7 |
| 2.4 Robot Dynamics : 3-DOF Robot Leg | 9 |
| 3 Controller Design | 11 |
| 3.1 Position Control for 1-DOF Robot Arm | 11 |
| 3.2 Torque Control for SEA | 13 |
| 3.3 Position Control for 3-DOF Robot Leg | 15 |
| 3.3.1 Direct-drive Model | 15 |
| 3.3.2 Redundant Actuators | 17 |
| 4 Parameter Selection | 19 |
| 4.1 Parameters for QDD | 19 |
| 4.1.1 Objective Function Formulation | 20 |
| 4.1.2 Final Selection | 21 |
| 4.2 Parameters for SEA | 22 |
| 4.2.1 Trade-off Analysis | 23 |
| 4.2.2 Objective Function Formulation | 24 |
| 4.2.3 Final Selection of Gearbox and Spring | 25 |
| 4.2.4 Gain Choice for Torque Control | 26 |

| | | |
|----------|---|-----------|
| 4.2.5 | Final Selection | 27 |
| 5 | Implementation : 1-DOF Robot Arm | 29 |
| 5.1 | Parameter Overview | 29 |
| 5.2 | Test Results : Single Actuators | 30 |
| 5.3 | Redundant Actuation Design | 31 |
| 5.3.1 | Torque Distribution | 32 |
| 5.3.2 | Torque Tracking Performance | 36 |
| 5.4 | Test Results : Single and Redundant Actuators | 38 |
| 6 | Implementation : 3-DOF Robot Leg | 39 |
| 6.1 | Position Control : Redundant Actuator | 39 |
| 6.2 | Parameter Overview : Controller for 3-DOF Model | 40 |
| 6.3 | Test Results | 40 |
| 7 | Conclusions and Future Work | 43 |
| 7.1 | Review of Research Questions | 43 |
| 7.2 | Final Remark | 44 |
| 7.3 | Future Work | 45 |
| | References | 47 |
| | Appendices | |
| A | Mathematical Model for Leg Model | 49 |
| A.1 | Equations of Motions : Direct-drive | 49 |
| A.2 | Equations of Motions : Redundant Actuator | 51 |

Introduction

1.1 Problem Statement

In terms of manipulator design for robots, it is obvious that the simplest and most straightforward way to design actuators to ensure high performance in dynamic outputs, controllability and stability for position and force(torque) control is to use motors directly connected to robot joints. Assuming that intrinsic frictions (joint frictions, and viscous frictions of motors) can be negligible, direct-drive(DD) motor would be the most ideal type of actuator design because there is no mechanical loss from gear friction.

Practically speaking, however, it is not possible to adapt direct-drive actuators for manipulator-based robot designs, such as humanoids and quadruped robots. Motors of the DD actuators should deal with external loads as well as producing dynamic motions. Therefore, if the performance requirement is too high (high torque or high speed), they would be vulnerable to energy loss caused by Joule heating, which has a dominant influence on motor efficiency. The only way to tackle this issue is to choose more powerful motors. However, this is not always possible because it usually leads to an increase in motor dimension (weights, volumes) which is not ideal for the robot designs stated above. In this sense, a main problem that engineers should take into account is “what is a proper way to satisfy high performance in terms of system outputs and controllability, as well as minimizing reduction in motor efficiency?”.

In order to improve motor efficiency, quasi-direct-drive(QDD) and series-elastic actuators(SEA) have been widely used. Seeing from the expression “quasi”, QDD is an actuator set consisting of a gearbox with low reduction ratio and high torque motor. Applying low gear ratio, it leads to reduced reflection of inertia, fast response, and high motion/force control bandwidth comparable to DD. Also, low reduction means

that mechanical loss caused by transformation can be minimized properly. Seok et al.(2012) introduced an energy-efficient actuator design for fast and high-force leg motions of a quadruped robot. [1] The proprioceptive actuator design was implemented to the robot called MIT Cheetah, [2], and its performance in impact reduction and physical interaction was improved. [3] Also, thanks to high backdrivability, QDD has been regarded as a good choice for designing robots used for supportive tasks such as exoskeletons. Yu et al.(2020) introduced a soft exoskeleton design for patients having knee injury. [4]. However, due to the low gear ratio transmission, QDD has a limited torque capacity (maximum or permissible torque), which is also shown in DD motors.

In the case of SEA, it is a motor-and-gearbox set connected to joints with compliant elements, spring. It consists of a gearbox with high gear ratio, and middle-powered motor. The main purpose of this combination is to produce an elastic force(torque) by deforming the connected elastic element(spring) and to use it as an actuation force(torque) for motions. Due to relatively high gear reduction and compliance coupling, motor heating is considerably low compared to QDD, meaning that it would be competitive in terms of energy efficiency. Pratt and Williamson et al. (1995) first came up with this innovative conceptual design [5], and there have been many modifications and improvements and they have been implemented to energy-efficient actuator designs. Despite this strong merit, motion/force control bandwidth is relatively low, meaning that control system design would be complicated, and it is not easy to find out an optimal combination of physical parameters. (motors, gearboxes, and springs) In short, neither of the two types of actuators can be an ultimate and optimal actuator design for robots.

1.2 Related Works

Among all the conceptual designs made for a powerful and efficient actuator, this paper focuses on a design made with multiple motor drives. Tsagarakis et al. (2013) introduced a compliant knee joint actuator design which resembles a structure of human leg with antagonistic muscles. This was designed for a 1-DOF squatting robot, and it has SEA as a main drive, and parallel-elastic actuator as a supportive drive. [6], [7], [8] This concept was implemented to a 3-DOF squatting leg robot by Roozing et al. (2019) and this mechanism showed improved energy efficiency as well as dynamic performance, compared to single SEA-actuated robots. [9] Besides, Roozing et al. (2017) introduced a noble guideline of optimal stiffness selection for SEA using impedance rendering. [10] As another approach for choosing SEA spring stiffness, Edgar et al. (2019) showed a method to select proper spring stiffness for

minimal energy consumption of motors. [11] As for QDD, Grandesso et al. (2021) came up with a redundant actuator design consisting of QDD and SEA, and techniques for parameter selection using co-design was also introduced. [12]

1.3 Contributions

Similar to the work by Grandesso et al. (2021) [12], this paper deals with a redundant actuator, consisting of QDD and SEA, and corresponding control system designs. In this work, off-the-shelf motors and gearboxes were only concerned. This means that mechanical design for the components is beyond the scope of this work. Compared to the related works shown above, this work has the following contributions.

- **As the first main part of this paper, the whole procedure of actuator parameter selection for each design (QDD and SEA) is covered in detail from top to bottom.**
- **All the types of actuators including DD as a reference are compared in terms of several performance criteria; position tracking, joint torques, and energy consumption which is the main topic of this work.**
- **As the second part of this paper, a redundant actuator design consisting of QDD and SEA will be introduced, and its performance will be assessed through simulations to see how well it takes advantage of the positive aspects and mitigates negative ones of each type of actuators, and how beneficial it would be, compared to single DD actuators.**

1.4 Research Questions

This paper will mainly answer the following research questions below.

- **What are the possible drawbacks that single actuators (QDD and SEA) cannot overcome?**
- **How to combine the concepts of both QDD and SEA to take advantage of the benefits and mitigate the disadvantages of each type?**
- **Which criteria are required for system parameter selection? How can the optimal system parameters be chosen in a mathematical way?**
- **How to design actuation control systems for all the actuator dynamics which are nonlinear?**
- **How to evaluate the proposed design?**

1.5 Report Layout

In Chapter 2, all the types of actuators will be reviewed briefly. Next, mathematical models for friction terms caused by motors, gearboxes and joints, and motion dynamics for all the types of actuators will be shown; DD, QDD, SEA and redundant model. Next, the procedure of controller design will be introduced in Chapter 3.

As the first part of this paper, all the steps for actuator parameter selection will be discussed in Chapter 4. Next, the obtained parameters and controller settings will be implemented to a 1-DOF robot arm, and tracking performance and energy efficiency of the three types will be compared using simulations in Chapter 5. And, as the second part of the paper, the idea of redundant actuator will be introduced and its performance will be evaluated with simulations.

All in all, all the actuators including the proposed design will be implemented to a 3-DOF robot leg and tested in Chapter 6. Finally, all the research questions stated will be answered in Chapter 7 to summarize all the points and conclude this work. And, possible future work will also be shown.

Modelling

2.1 Types of Actuators

Figure 2.1 shows all the types of the actuator designs connected to rigid links weighing $1kg$, and having $0.03kg \cdot m^2$ of inertia. It is assumed that there is no friction on the joints, meaning that frictions will only be dependent on motors and gearboxes.

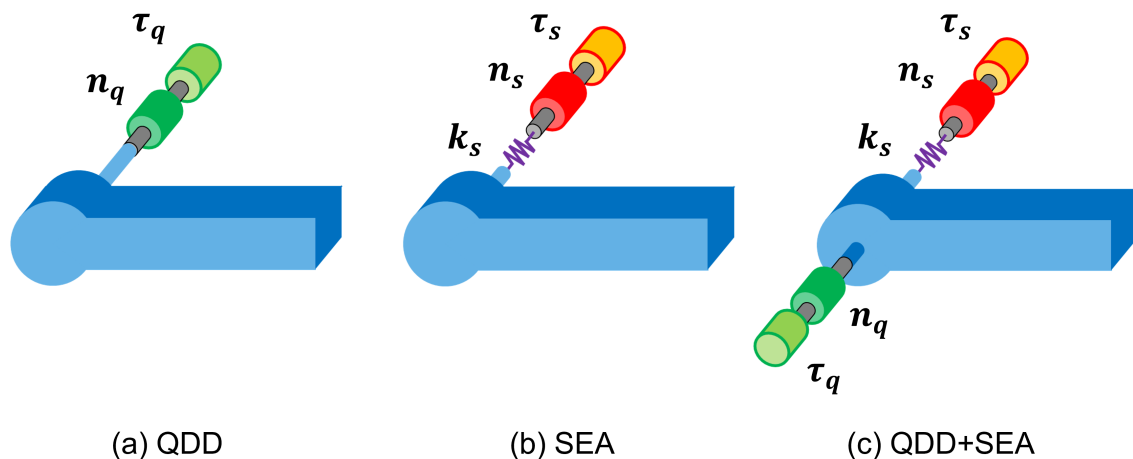


Figure 2.1: Types of Actuator Designs

As for DD actuator, a powerful motor without gearbox will be chosen. This is a reference used for comparison with the actuators stated above. A main goal is to make the weights of all the actuators lighter than or equal to the reference. When it comes to parameter selection, 1-DOF robot arm model, which is the same as pendulum model, will be considered for simplicity. Once all the parameters of each actuator design are chosen, they will be implemented in the leg model, after their performances are verified by simulations.

2.2 Frictions

For motor and gearbox selection, Maxon EC flat series and GP series will be considered as the candidates for motors and gearboxes. This section will explain how the friction model can be made from the given physical parameters. According to the key information manual, motor friction can be modelled with the given torque constant and no-load current as follows. Using the calculated friction torque, friction coefficient can also be obtained using the given no-load speed, ω_{nl} . [13]

$$\tau_f = K_t \cdot I_{nl} = B \cdot \omega_{nl} \quad (2.1)$$

The relation between stall torque and no-load speed of motor can be shown as a speed-torque curve. [14] If the gearbox is ideal, input and output powers should be the same. However, this is not possible due to the friction torque, $\tau_{g,f}$ made by gearboxes.

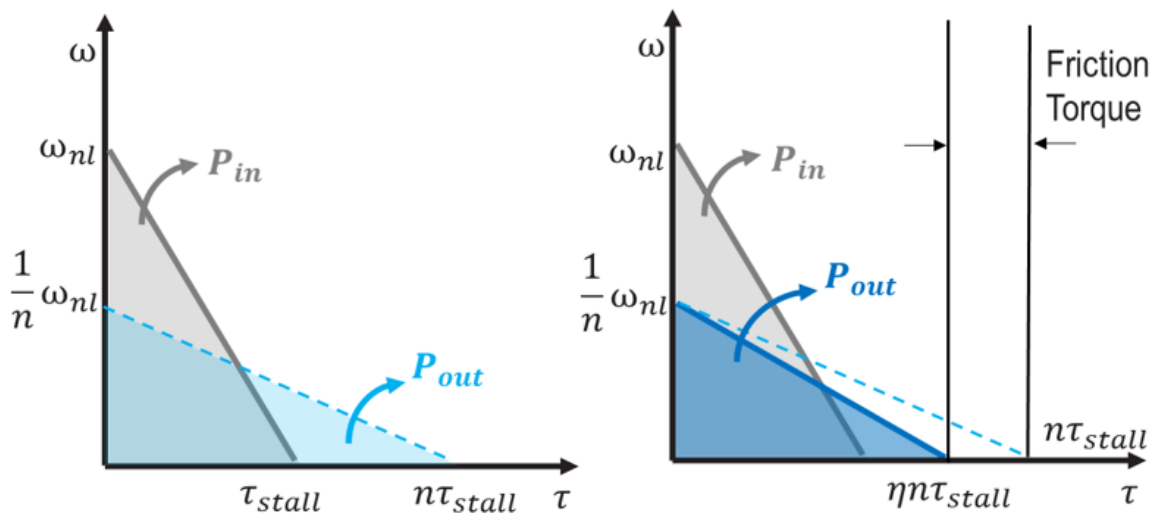


Figure 2.2: Speed-torque Curve for Ideal(left) and General(right) Cases

The figure shows that gearbox efficiency, η can be used to model the gear friction as follows. These two coefficients can be used in the robot dynamics as the lumped friction terms.

$$B_g = \frac{\tau_{g,f}}{\omega_{nl}} = \frac{(1 - \eta)\tau_{stall}}{\omega_{nl}} \quad (2.2)$$

2.3 Robot Dynamics : 1-DOF Robot Arm

First, equation of motion for direct-drive actuator is as follows. It is noted that joint friction, f_v is zero.

$$(I_l + J_r)\ddot{q}_l + (f_v + B_r)\dot{q}_l + m_l g d_l \cos q_l = \tau_l \quad (2.3)$$

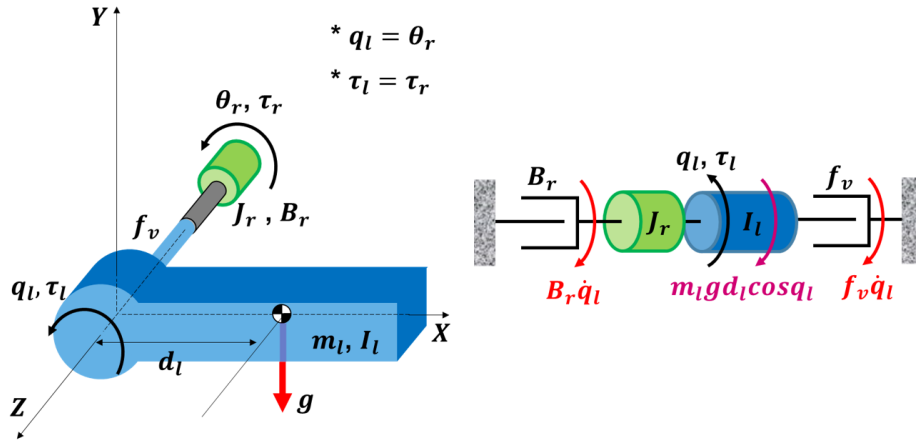


Figure 2.3: Robot Dynamics for DD

Second, dynamics for quasi-direct-drive actuator is as follows. This is an equivalent form consisting of the reflected inertial and damping terms.

$$[I_l + n_q^2(J_q + J_{g,q})]\ddot{q}_l + [f_v + n_q^2(B_q + B_{g,q})]\dot{q}_l + m_l g d_l \cos q_l = \tau_{l,q} \quad (2.4)$$

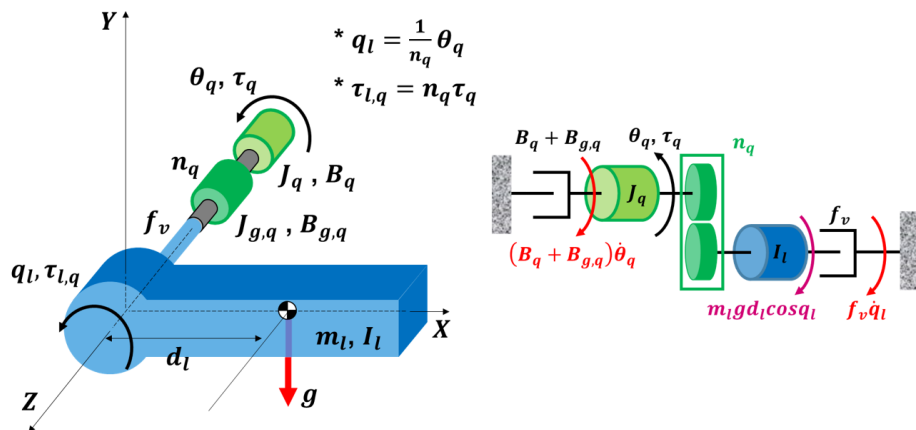


Figure 2.4: Robot Dynamics for QDD

Next, dynamics for series-elastic actuator are as follows. Due to the compliance between the gearbox and link shafts, elastic torque is added in the equations.

$$(J_s + J_{g,s})\ddot{\theta}_s + (B_s + B_{g,s})\dot{\theta}_s + \frac{1}{n_s}k_s \left(\frac{1}{n_s} - q_l \right) = \tau_s \quad (2.5)$$

$$I_l \ddot{q}_l + f_v \dot{q}_l + m_l g d_l \cos q_l = k_s \left(\frac{1}{n_s} \theta_s - q_l \right) \quad (2.6)$$

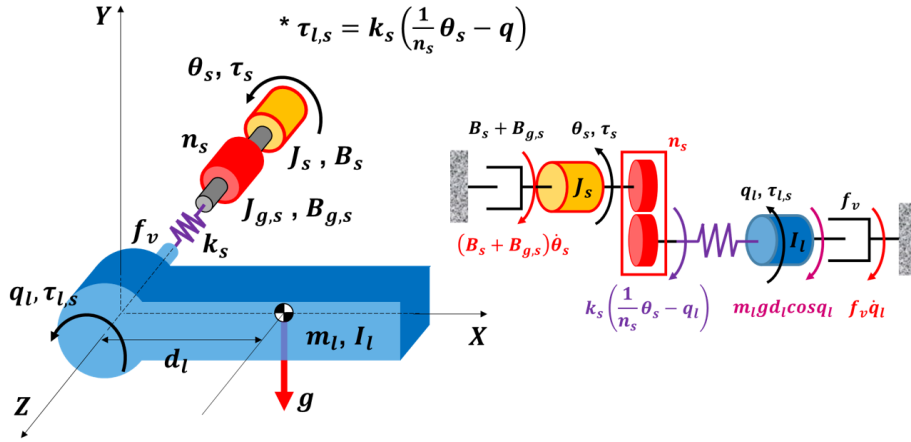


Figure 2.5: Robot Dynamics for SEA

Finally, mathematical models for redundant case (QDD and SEA) are as follows.

$$(J_s + J_{g,s})\ddot{\theta}_s + (B_s + B_{g,s})\dot{\theta}_s + \frac{1}{n_s}k_s \left(\frac{1}{n_s} \theta_s - q_l \right) = \tau_s \quad (2.7)$$

$$[I_l + n_q^2(J_q + J_{g,q})]\ddot{q}_l + [f_v + n_q^2(B_q + B_{g,q})]\dot{q}_l - k_s \left(\frac{1}{n_s} \theta_s - q_l \right) + m_l g d_l \cos q_l = \tau_{l,q} \quad (2.8)$$

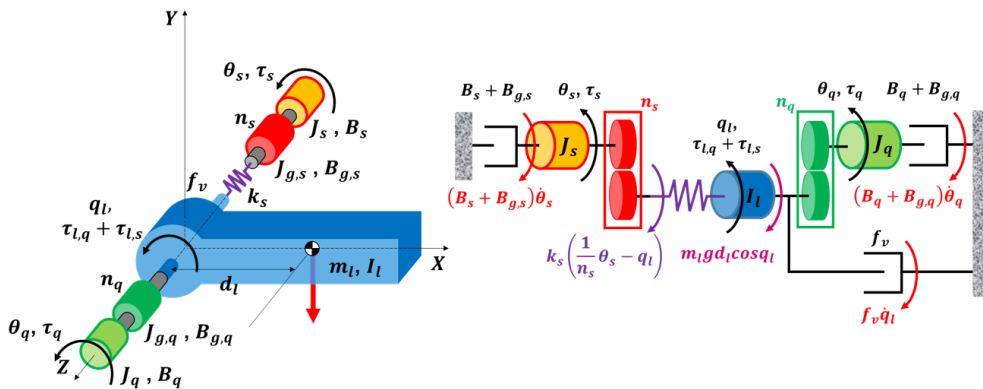


Figure 2.6: Robot Dynamics for QDD and SEA

2.4 Robot Dynamics : 3-DOF Robot Leg

To formulate the equations of motions, Euler-Lagrangian method can be used. [15] Including the friction terms, joint torques can be calculated as follows.

$$\tau_l^* = \frac{\partial}{\partial t} \left(\frac{\partial L}{\partial \dot{q}} \right) - \frac{\partial L}{\partial q} + \frac{\partial D}{\partial \dot{q}}, \quad (2.9)$$

where L is Lagrangian which is $L = K - P$, K and P are lumped kinetic and potential energy terms, and D is a lumped dissipated energy made by motor and gearbox frictions. Eq. 2.9 can be formulated into a matrix form, consisting of inertial, centrifugal, Coriolis, friction terms and a lumped term of elastic and gravitational torques. Each term was expressed as M , C , Co , D , and G , respectively.

$$M(q)\ddot{q} + C(q)\dot{q}^2 + Co(q)\dot{q}\dot{q} + D\dot{q} + G(q) = \tau_l^* \quad (2.10)$$

The following figure shows a simplified schematic of 3-DOF robot legs. Since it will only make vertical motions, mathematical model of the robot leg can be modelled by using a planar 3-DOF serial manipulator.

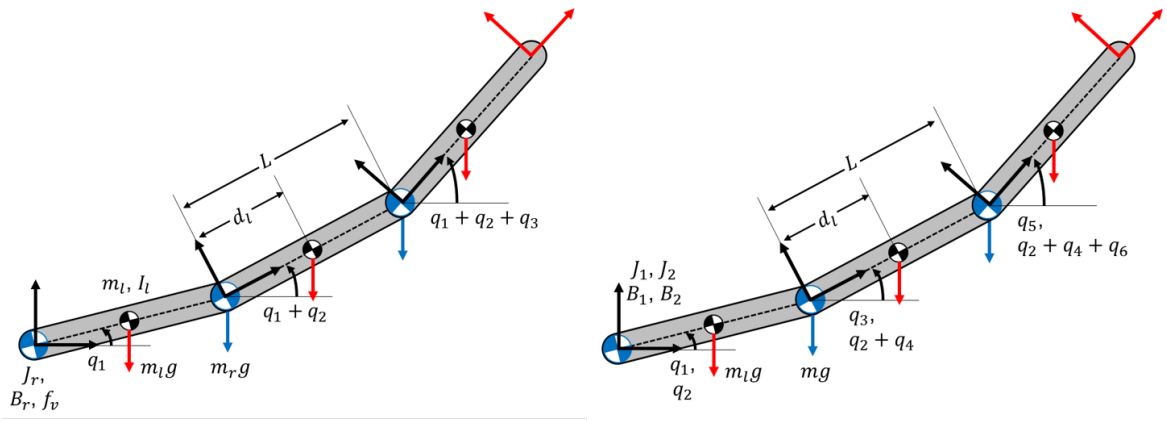


Figure 2.7: 3-DOF Robot Legs with DD and Redundant Actuators

The model on the left side is a leg model which uses DD as its actuators, and the right-side model uses redundant (QDD and SEA) actuators. As for the redundant model, since there are two actuators on a single joint, DOF of robot dynamics for a redundant model is supposed to be 6. To elaborate, there are two equations of motions for one link; SEA motor dynamics and link dynamics. The velocity product vectors for C and Co were defined as follows.

$$\ddot{q}_{dd}^2 = \begin{bmatrix} \dot{q}_1^2 \\ \dot{q}_2^2 \\ \dot{q}_3^2 \end{bmatrix}, \dot{q}\dot{q}_{dd} = \begin{bmatrix} \dot{q}_1\dot{q}_2 \\ \dot{q}_2\dot{q}_3 \\ \dot{q}_3\dot{q}_1 \end{bmatrix}, \ddot{q}_{red}^2 = \begin{bmatrix} \dot{q}_1^2 \\ \dot{q}_2^2 \\ \dot{q}_3^2 \\ \dot{q}_4^2 \\ \dot{q}_5^2 \\ \dot{q}_6^2 \end{bmatrix}, \text{ and } \dot{q}\dot{q}_{red} = \begin{bmatrix} \dot{q}_1\dot{q}_3 \\ \dot{q}_2\dot{q}_4 \\ \dot{q}_3\dot{q}_5 \\ \dot{q}_4\dot{q}_6 \\ \dot{q}_5\dot{q}_1 \\ \dot{q}_6\dot{q}_2 \end{bmatrix} \quad (2.11)$$

As the right side of Figure 2.7 shows, the odd-numbered angles of the redundant model (q_1 , q_3 and q_5) represent SEA motor angles, and even-numbered ones are angles of the joints. This is because the first equations of motions for each link is related to SEA, the second ones are about links and QDD motors. In this way, odd-numbered rows of equations are for SEA, and even-numbered ones are for the others. Symbolic notations and mathematical formulations for each model are summarized in Appendix A.

Controller Design

There are two controllers; position controller of all the cases (outer loop), and torque controller for SEA (inner loop). Roozing et al. 2017 [10] introduced how controllers for non-linear dynamics can be designed using pole placement technique. Using this idea, control gains for position and torque controllers will be chosen using linearized robot dynamics.

3.1 Position Control for 1-DOF Robot Arm

Position controller can be designed using the direct-drive dynamics with the structure shown below. From the typical PD controller, derivative of the trajectory was omitted. This makes the closed-loop system do not have zero, resulting in stability.

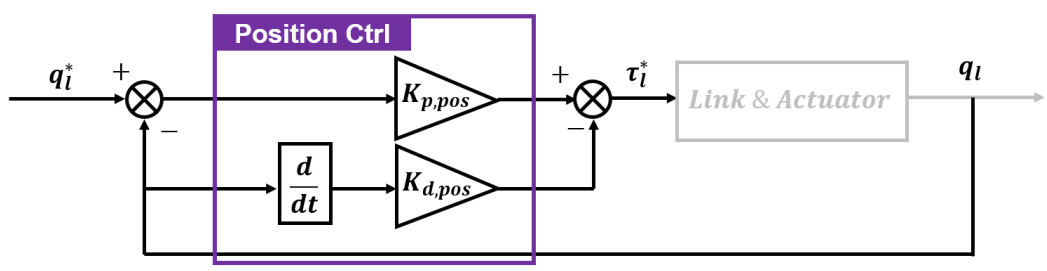


Figure 3.1: Block Diagram of Position Controller

It is assumed that the arm makes a rotation close to an equilibrium angle $q_{eq} = -90^\circ$. According to trigonometric relation, Eq. 2.3 can be transformed as follows.

$$I\ddot{q}_{eq} + d\dot{q}_{eq} + k\cos q_{eq} = I\ddot{q}'_{eq} + d\dot{q}'_{eq} + k\sin q'_{eq} = \tau_l, \quad (3.1)$$

where $I = I_l + J_r$, $d = B_r$, $k = m_l g d_l$ and $q'_{eq} = 90^\circ + q_{eq}$.

Applying Laplace transform, Eq. 3.1 can be linearized as follows.

$$(Is^2 + ds + k)\theta(s) = \tau_l(s), \quad (3.2)$$

As for the motor, Maxon EC 90 flat (No.597976) model was chosen. Parameters are summarized in Table 3.1.

| Motor | | | | | | |
|--------------|----------------|-------------|-----------------------------|------------------|----------------|----------------|
| Power | Voltage | Mass | Inertia | Friction | ω_{nl} | τ_{stall} |
| [W] | [V] | [kg] | [kg · m²] | [Nms/rad] | [rad/s] | [Nm] |
| 600 | 60 | 0.988 | 5.06E-04 | 3.17E-04 | 207.35 | 13.3 |

Table 3.1: Chosen DD Motor Parameters

Referring to Figure 3.1, closed-loop transfer function can be formulated as follows.

$$H_{r/y} = \frac{K_p}{Is^2 + (d + K_d)s + (k + K_p)} \quad (3.3)$$

Using the pole placement techniques shown by Roozing et al. (2017) [10] with the linearized model, ratio of open-loop and closed-loop frequencies, $\alpha = \omega_{cl}/\omega_n$ can be defined. In the meantime, closed-loop characteristic polynomial can be rearranged as follows.

$$s^2 + \frac{d + K_d}{I}s + \frac{k + K_p}{I} = s^2 + 2\zeta\omega_{cl}s + \omega_{cl}^2 \quad (3.4)$$

For simplicity, critical damping condition ($\zeta = 1$) was chosen for this controller. Substituting α and solving the equation with respect to K_p and K_d , yields

$$K_p = k(\alpha^2 - 1), K_d = 2I\omega_{cl} - d = 2I\alpha\sqrt{\frac{k}{I}} - d \quad (3.5)$$

The idea is to find out the optimal control gains by changing closed-loop pole locations with α . For simulations, the following reference profile was used.

$$q_i^*(t) = \frac{\pi}{2} \sin 2\pi ft, \quad (3.6)$$

where $f = 2Hz$ is a motion bandwidth.

A set of α ranging from 1.1 to 49.1 was used. And, root mean square of the output errors was used for analysis. Shown from the left of Figure 3.2, larger α would be preferred to minimize error. However, it is noted that control gains should not be unnecessarily high. When α was chosen as 17.1, error decreased to about $0.2rad$. This is mainly due to the phase difference between the reference and output. As the right side shows, this phase shift became less than $20ms$, which is acceptable. Therefore, $\alpha = 17.1$ was selected as a final value. As a result, control gains were calculated as $K_p = 428.81$, and $K_d = 7.25$.

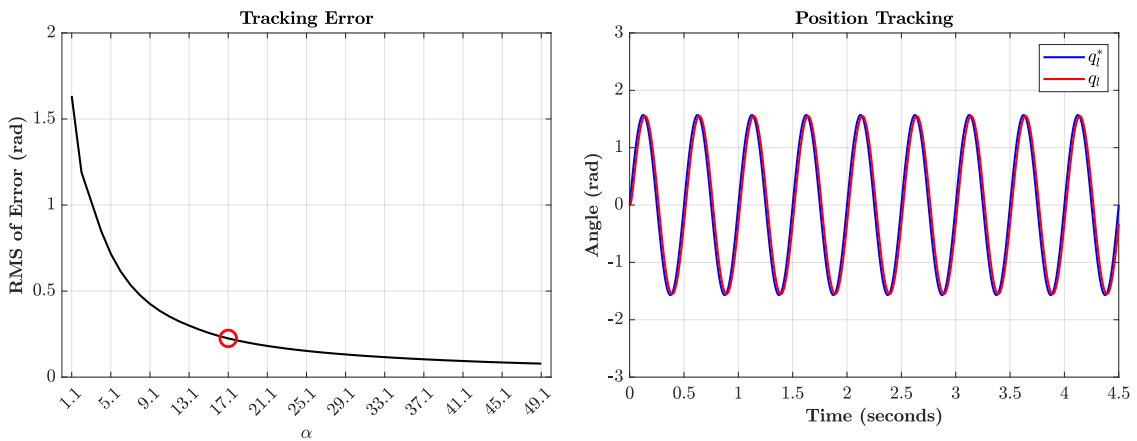


Figure 3.2: Test Results of Gain Tuning Simulations

3.2 Torque Control for SEA

Unlike the case of DD or QDD that are rigidly connected to the joint, SEA is connected with a compliant element. The resultant joint torque that SEA produces can be expressed as follows.

$$\tau_{l,s} = k_s \left(\frac{1}{n_s} \theta_s - q_l \right) \tag{3.7}$$

Due to the compliance coupling, SEA is vulnerable to stability when high frequency motions or forces are applied. In order to tackle this issue, additional torque controller can be used, as well as feedforward term. This can be shown as follows.

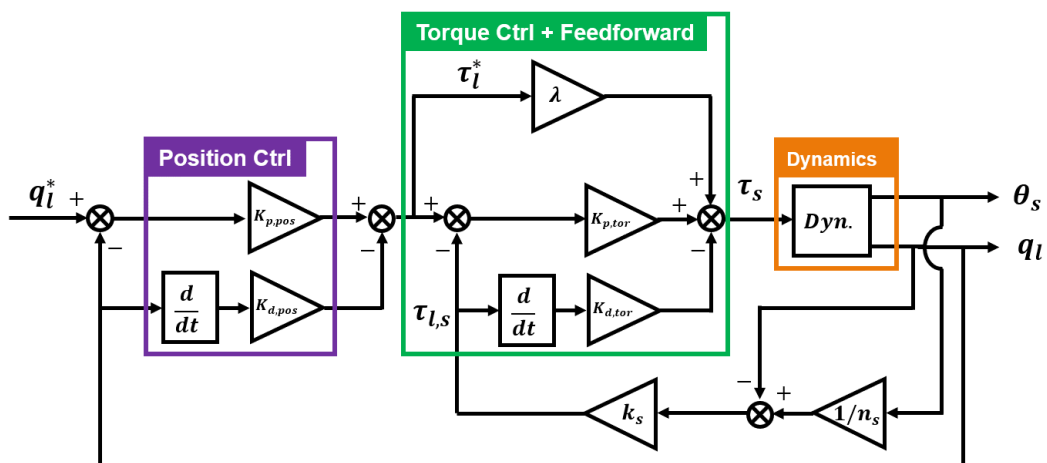


Figure 3.3: Block Diagram of SEA Torque Controller

Using this system structure, control input, τ_s can be formulated as follows.

$$\tau_s = (K_p + K_d s + \lambda)\tau_l^*, \quad (3.8)$$

where τ_l^* is the desired joint torque. Applying Laplace transform and substituting the control input into Eq. 2.5 , yields

$$(K_p + K_d s + \lambda)\tau_l^* = (nJs^2 + nBs)q_l(s) + \left[nJs^2 + (nB + kK_d) + \left(\frac{k}{n} + kK_p \right) \right] \left[\frac{1}{n}\theta_s(s) - q_l(s) \right], \quad (3.9)$$

where J and B are lumped inertia and damping of SEA motor and gearbox, n and k are gear ratio and spring stiffness. Using the definition of α and critical damping ratio ($\zeta = 1$), control gains for the controller can be formulated as follows.

$$K_p = \frac{1}{n}(\alpha^2 - 1), K_d = \frac{2\alpha\sqrt{kJ} - nB}{k} \quad (3.10)$$

From the list of candidates, 3 gearboxes and 3 springs were chosen, which are the minimum, median, and maximum values in the list. Using these parameters, similar simulations were done with varying α .

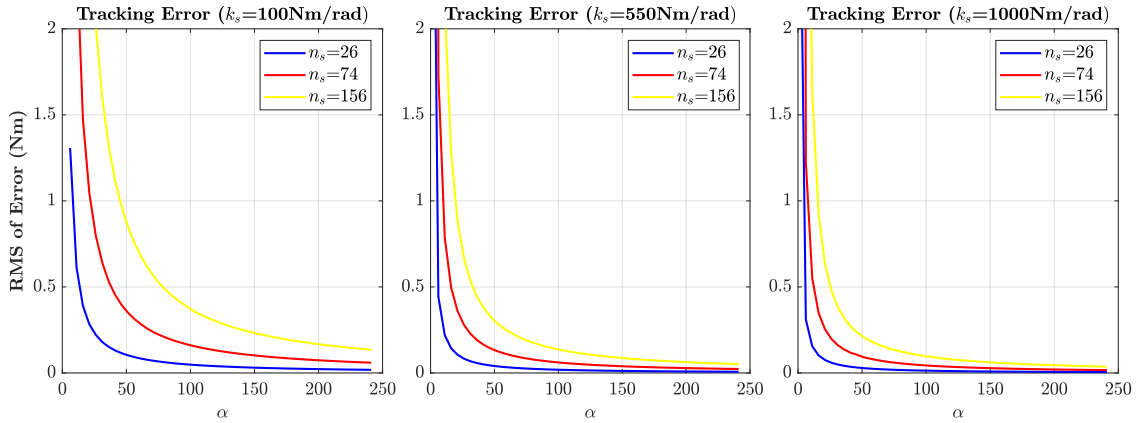


Figure 3.4: Gain Tuning Simulations, with Different Gearboxes and Springs

It is clear that errors will decrease as α increases. And, when the gear ratio is relatively high, much higher α is needed to reduce errors. In addition, when the spring stiffness is high, much lower α suffices. Due to uncertainty of final optimal choice of spring and gearbox, $\alpha = 100$ was first chosen, considering that it showed quite a descent level of error at all parameter combinations. This can be used for SEA parameter selection. And, if the control gains are unnecessarily high, lower α can also be found to lower the gains. This will be done at the end of SEA optimization in the next chapter.

3.3 Position Control for 3-DOF Robot Leg

The same idea used in the 1-DOF position controller design was used for 3-DOF controller as well.

3.3.1 Direct-drive Model

Neglecting velocity product terms, Eq. 2.10 can be simplified as follows.

$$\begin{bmatrix} m_{11} & m_{12} & m_{13} \\ m_{21} & m_{22} & m_{23} \\ m_{31} & m_{32} & m_{33} \end{bmatrix} \begin{bmatrix} \ddot{q}_1 \\ \ddot{q}_2 \\ \ddot{q}_3 \end{bmatrix} + \begin{bmatrix} d_{11} & d_{12} & d_{13} \\ d_{21} & d_{22} & d_{23} \\ d_{31} & d_{32} & d_{33} \end{bmatrix} \begin{bmatrix} \dot{q}_1 \\ \dot{q}_2 \\ \dot{q}_3 \end{bmatrix} + \begin{bmatrix} G_1(q) \\ G_2(q) \\ G_3(q) \end{bmatrix} = \begin{bmatrix} \tau_1 \\ \tau_2 \\ \tau_3 \end{bmatrix} \quad (3.11)$$

Suppose that all the joint angles are so minute. Then, input torques for each joint do not affect the outputs of other joints, meaning that three dynamics can be regarded as an independent set of equations. In this sense, off-diagonal elements inside M and D matrices can be neglected, and Eq. 3.11 can be written as follows.

$$\begin{bmatrix} m_{11} & 0 & 0 \\ 0 & m_{22} & 0 \\ 0 & 0 & m_{33} \end{bmatrix} \begin{bmatrix} \ddot{q}_1 \\ \ddot{q}_2 \\ \ddot{q}_3 \end{bmatrix} + \begin{bmatrix} d_{11} & 0 & 0 \\ 0 & d_{22} & 0 \\ 0 & 0 & d_{33} \end{bmatrix} \begin{bmatrix} \dot{q}_1 \\ \dot{q}_2 \\ \dot{q}_3 \end{bmatrix} + \begin{bmatrix} G_1(q) \\ G_2(q) \\ G_3(q) \end{bmatrix} = \begin{bmatrix} \tau_1 \\ \tau_2 \\ \tau_3 \end{bmatrix} \quad (3.12)$$

Since each actuator has different amount of loads at the ends of each link, it is clear that control gains should be chosen independently. Using the simplified equations and the same linearization and pole placement, control gains can be chosen for each link dynamics.

It is not easy to tune the gains for each joint at the same time. For simplicity, the following steps were done for gain choice for the controllers.

- **Step 1) Gains for Ankle Joint, with fixed Knee and Hip Joints**

First, gain tuning for the first joint can be done with other two fixed joints. Physically, it means that an ankle joint moves a link equivalent to all the links and actuators on the second and third joints. Gains can be found by simulations with varying frequency ratios, α .

- **Step 2) Gains for Knee Joint, with fixed Hip Joint**

Next, gain tuning for the second joint can be done with a fixed hip joint. Similarly, knee joint has a load equivalent to the sum of the second and third links

and actuator for a hip joint. Using the gains for ankle joint obtained from the previous step, gains can be found in the same way.

- **Step 3) Gains for Hip Joint**

Finally, gains for the hip joint can be tuned, using the actual dynamics and all the gains obtained from the two steps.

For simulations, motion profiles shown in Figure 3.5 were used. It shows briefly how the squatting motion will be made per cycle. And, in order to validate the performance with different conditions, this will be tested with three different speeds.

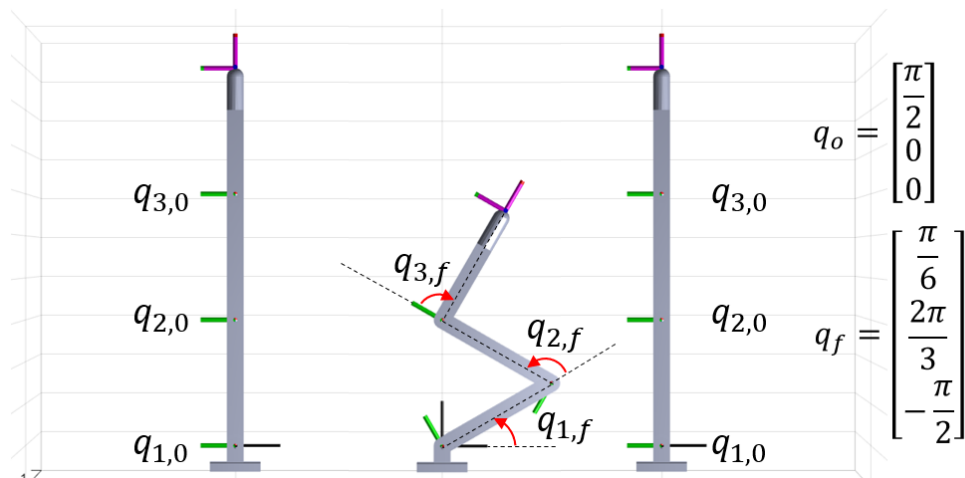


Figure 3.5: Schematic of Squatting Motion Profile per Cycle

In this case, a set of α ranging from 1.1 to 10.1 was used. As Figure 3.6 shows, [7.1, 7.6, 5.6] were chosen as α values for each joint.

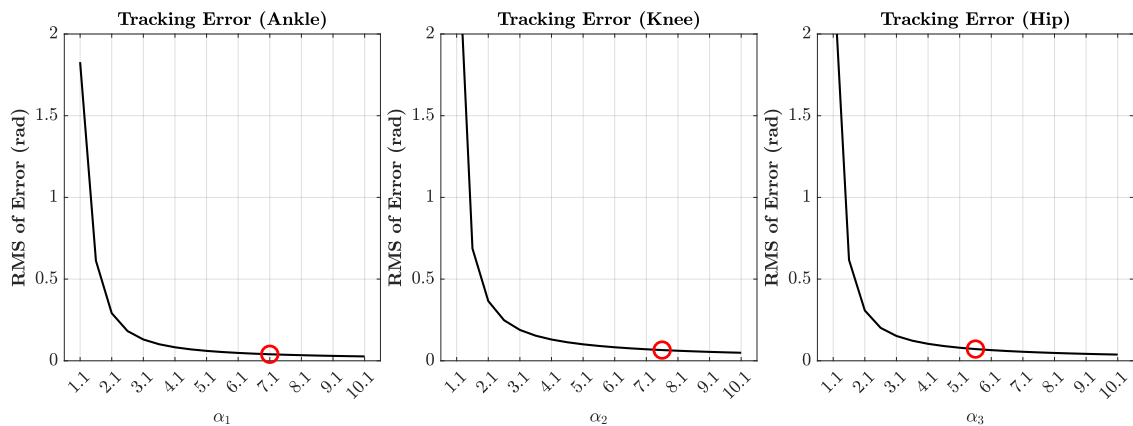


Figure 3.6: Test Results of Gain Tuning Simulations

This is because the chosen α values are the minimums that make the system output have less steady-state errors, and peaks at the starting points of steady-state regions shown in the middle of the cycles.

As stated above, Figure 3.7 shows how the joints track the motion trajectories with low, medium and high frequencies, and how much the resultant joint torques are needed. Although a minor phase shift can be seen from the upper plots, this can be said to be acceptable because it is about 50 ms.

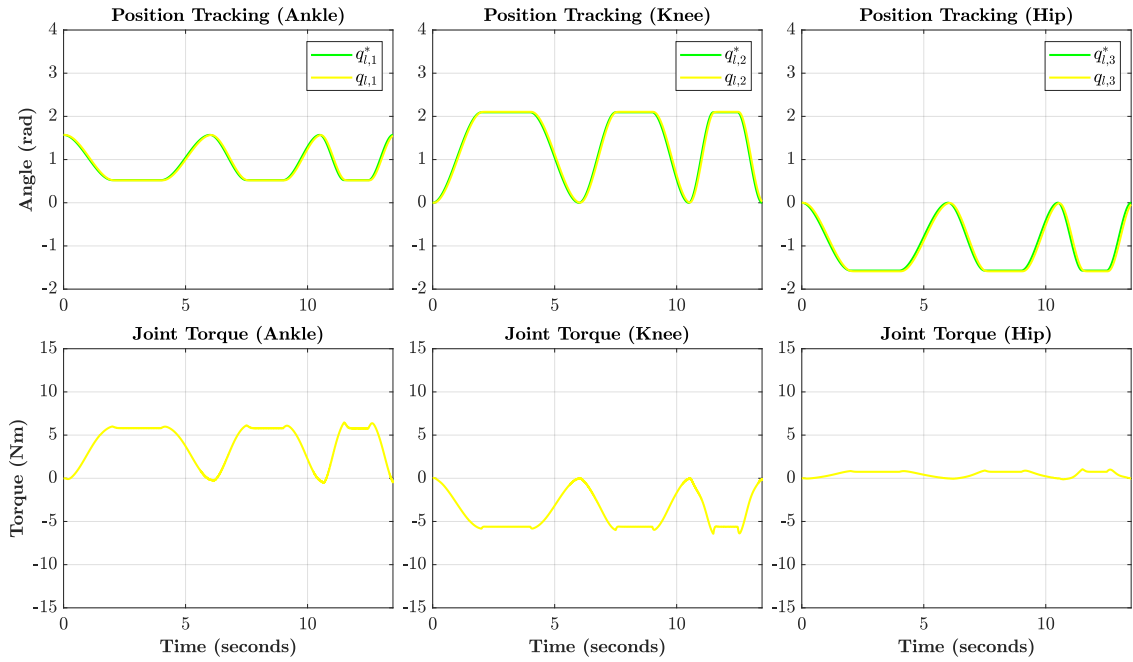


Figure 3.7: Position Tracking(Upper) and Joint Torques (Lower) for DD Actuators

3.3.2 Redundant Actuators

As explained in Appendix A.2, while odd-numbered rows of equations are SEA motor dynamics, even-numbered ones represent QDD and link dynamics. In order for position controller design, link dynamics are required. The same technique shown for the DD case simplifies the link dynamics for redundant design as follows.

$$\begin{bmatrix} m'_{22} & 0 & 0 \\ 0 & m'_{44} & 0 \\ 0 & 0 & m'_{66} \end{bmatrix} \begin{bmatrix} \ddot{q}_2 \\ \ddot{q}_4 \\ \ddot{q}_6 \end{bmatrix} + \begin{bmatrix} d'_{22} & 0 & 0 \\ 0 & d'_{44} & 0 \\ 0 & 0 & d'_{66} \end{bmatrix} \begin{bmatrix} \dot{q}_2 \\ \dot{q}_4 \\ \dot{q}_6 \end{bmatrix} + \begin{bmatrix} G'_2(q) \\ G'_4(q) \\ G'_6(q) \end{bmatrix} = \begin{bmatrix} \tau_2 \\ \tau_4 \\ \tau_6 \end{bmatrix}, \quad (3.13)$$

where a superscript 'prime' indicates "redundant" dynamics.

The process for gain tuning can be done with the same method shown in DD position controller design. However, this can be done once all the design specifications for the redundant actuators are determined. In the next chapter, actuator parameters for QDD and SEA will be selected. In Chapter 5, a design strategy of redundant actuator will be introduced, and the design will be finalized using the chosen parameters. Then, gain choice for position controllers of this actuator model will be done in the beginning of Chapter 6.

Parameter Selection

Except for DD parameters, motors and gearboxes of QDD and SEA, and SEA spring stiffness will be selected by the optimization process. As stated in the previous chapter, inertia and friction coefficient of DD were chosen as $J_r = 5.06 \times 10^{-4} \text{kg} \cdot \text{m}^2$, and $B_r = 3.17 \times 10^{-4} \text{Nms/rad}$.

4.1 Parameters for QDD

As shown in the table below, there are 64 possible pairs of motors and gearboxes in total. Through the parameter optimization, all the possible variations will be tested and compared with one another, so that the best combination in terms of performance targets can be found.

| No. | Motor | | | | | | | Gearhead | | | |
|-----|--------------|----------------|--------------|-----------------------------------|-----------------------|--------------------------|------------------------|--------------|-----------------------------------|--------------|-------------------|
| | Power [W] | Voltage [V] | Mass [kg] | Inertia [kg · m ²] | Friction [Nms/rad] | ω_{nl} [rad/s] | τ_{stall} [Nm] | Mass [kg] | Inertia [kg · m ²] | Ratio [-] | Efficiency [-] |
| 1 | 60 | 18 | 0.1131 | 1.35E-05 | 1.36E-05 | 601.09 | 1.19 | 0.26 | 1.40E-06 | 3.5 | 0.90 |
| 2 | 90 | 18 | 0.1151 | 1.35E-05 | 1.38E-05 | 601.09 | 1.19 | 0.26 | 9.10E-07 | 4.3 | 0.90 |
| 3 | 60 | 48 | 0.1131 | 1.35E-05 | 1.36E-05 | 601.09 | 1.04 | 0.26 | 4.90E-07 | 6.0 | 0.90 |
| 4 | 90 | 48 | 0.1151 | 1.35E-05 | 1.37E-05 | 601.09 | 1.04 | 0.36 | 1.50E-06 | 12.0 | 0.81 |
| 5 | 120 | 24 | 0.1491 | 1.81E-05 | 1.91E-05 | 586.43 | 1.69 | 0.36 | 1.50E-06 | 15.0 | 0.81 |
| 6 | 120 | 36 | 0.1491 | 1.81E-05 | 1.87E-05 | 620.99 | 1.32 | 0.36 | 9.40E-07 | 19.0 | 0.81 |
| 7 | 120 | 48 | 0.1491 | 1.81E-05 | 1.91E-05 | 584.34 | 1.26 | 0.36 | 1.40E-06 | 21.0 | 0.81 |
| 8 | 120 | 60 | 0.1491 | 1.81E-05 | 2.27E-05 | 389.56 | 1.24 | 0.36 | 9.10E-07 | 26.0 | 0.81 |

Table 4.1: Candidates of QDD Motors and Gearboxes

4.1.1 Objective Function Formulation

The following objective function shows the costs which should be minimized.

$$E = \sum_{i=1}^3 W_i E_i = W_1 E_1 + W_2 E_2 + W_3 E_3 \quad (4.1)$$

- **E_1) Reflected inertia, $n_q^2(J_q + J_{g,q})$**
Minimal reflected inertia makes the system have higher motion bandwidth. This is the main concept of QDD design, consisting of high torque motor and low gear reduction.
- **E_2) Friction Loss, $\int [f_v + n_q^2(B_q + B_{g,q})] \dot{q}_l^2 dt$**
Grandesso et al. 2021 [12] considered mechanical power consumption in the cost function. However, in this work, energy loss caused by friction is mainly concerned.
- **E_3) Heat Loss, $\int (\tau_q / K_{t,q})^2 R_{m,q} dt$**
For actuators with low gear ratio, most of the energy losses are caused by Joule heating of motor. [8]
- **W_i) Scaling factor, $w_i / \text{Min}(E_i)$**
Since each cost has their own different ranges, the calculated data should be normalized. By dividing costs with $\text{Min}(E_i)$, all the costs can be put into the range from 1 to their own maximum values. As for weighting factors, heat loss minimization is the most, and reflected damping minimization is the least important ones. Thus, weights were selected as $w_i = [w_1, w_2, w_3] = [0.3, 0.2, 0.5]$.

All in all, conditions for simulations are summarized as follows. As for E_2 and E_3 , motor torque and velocity from simulations should be filtered to prevent from irregular peaks or noise. In this case, moving average filter was used, with a 2Hz-sized window.

- $q_l^*(t) = 0.5\pi \sin 2\pi ft$, and $f = 2Hz$, $t = [0, 5]sec$,
- $E_1 = n_q^2(J_q + J_{g,q})$, and $W_1 = 0.3 / \text{Min}(E_1)$
- $E_2 = \int [f_v + n_q^2(B_q + B_{g,q})] \dot{q}_l^2 dt$, and $W_2 = 0.2 / \text{Min}(E_2)$
- $E_3 = \int (\frac{\tau_q}{K_{t,q}})^2 R_{m,q} dt$, and $W_3 = 0.5 / \text{Min}(E_3)$

4.1.2 Final Selection

The following figure shows the colormaps plotted with the calculated costs.

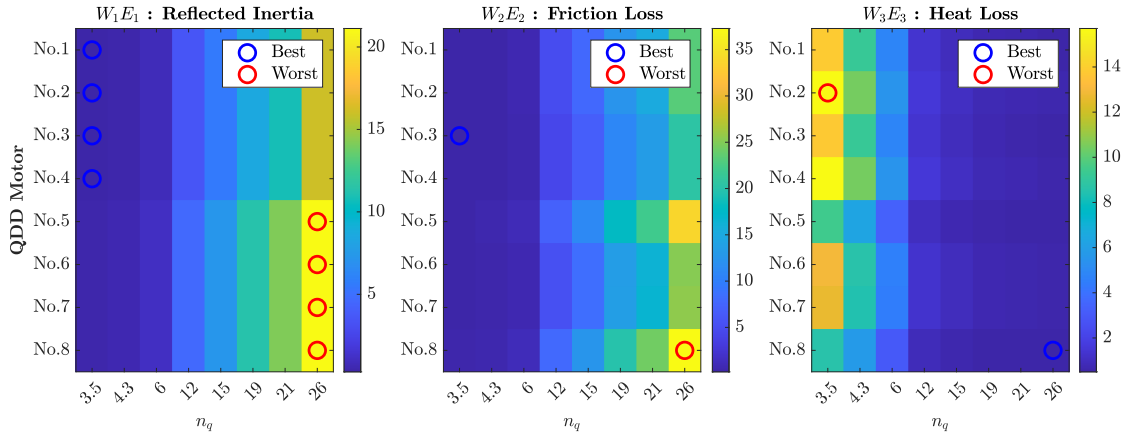


Figure 4.1: Colormaps of Scaled Costs of QDD Optimization

As for W_1E_1 , 4 minimum and maximum values were shown. This is because every four motors have the same rotor inertia. Looking into W_3E_3 , it shows a different trend from those of W_1E_1 or W_2E_2 . This could be expected because minimizing gear ratio helps reducing reflected inertia or damping (friction loss), whereas motor heat would be high the gear ratio is too small.

As the left side of Figure 4.2 shows, minimized total cost can be obtained. Before finalizing optimization, the selected pair should be validated in terms of feasibility.

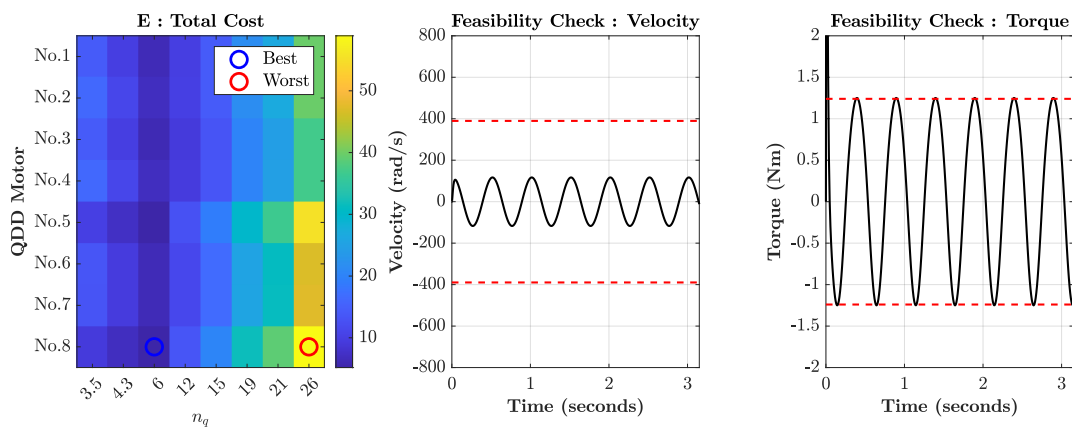


Figure 4.2: Feasibility Check of the Minimal Choice

To elaborate, motor has its own limitations of maximum torque and velocity. In this work, these limitations were set to stall torque and no-load speed of the chosen

motor. Through a final simulation, whether the selected motor operates within the maximum ranges. The right side of Figure 4.2 shows that the selected motor's torque exceeds the maximum range. Alternatively, the second best option was chosen for a safety purpose. Seeing that it satisfied both torque and speed limits, Maxon EC 45 flat (No.608148) motor and GP 42C (No.260551) gearbox were chosen.

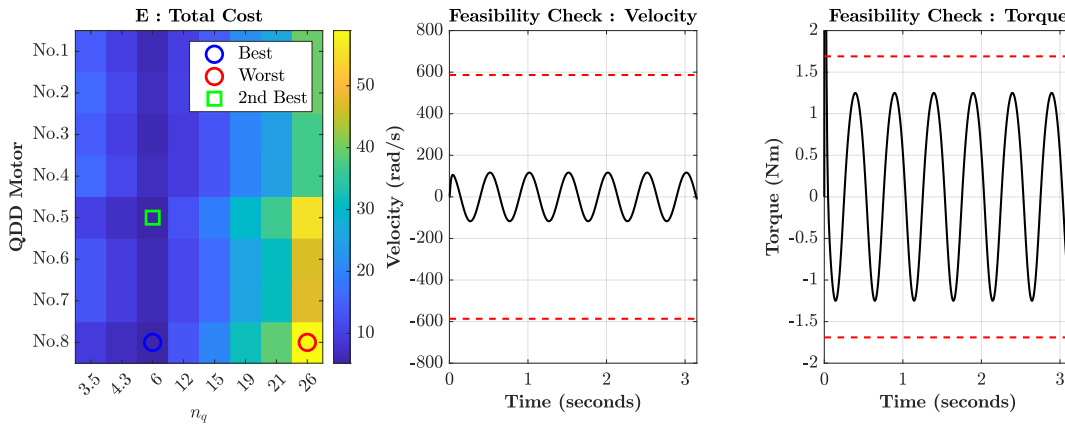


Figure 4.3: Feasibility Check of the Alternative Choice

| | | Motor | | | | | Gearhead | | | |
|-------|---------|--------|------------------------|------------|---------------|----------------|----------|------------------------|-------|------------|
| Power | Voltage | Mass | Inertia | Friction | ω_{nl} | τ_{stall} | Mass | Inertia | Ratio | Efficiency |
| [W] | [V] | [kg] | [kg · m ²] | [Nm/s/rad] | [rad/s] | [Nm] | [kg] | [kg · m ²] | [-] | [-] |
| 120 | 24 | 0.1491 | 1.81E-05 | 1.91E-05 | 586.43 | 1.69 | 0.26 | 4.90E-07 | 6.0 | 0.90 |

Table 4.2: Final Selection of QDD Motor and Gearbox

4.2 Parameters for SEA

Unlike those for QDD, there are three parameters to be selected.

- **Motor (J_s and B_s)**
- **Gearbox ($J_{g,s}$ and $B_{g,s}$)**
- **Spring Stiffness (k_s)**

To elaborate, 2-dimensional optimization (gearbox and spring) should be done for every motor candidate in the list, and the most ideal combination (motor, gearbox and spring) should be chosen as a final selected parameter set. If there are many motor candidates to choose from, completion time for SEA parameter optimization would be long because each iteration includes three simulations, which will

be shown later. For simplicity, it is assumed that the motor specification for SEA is fixed. Accordingly, Maxon EC 45 flat (No.608136) model was chosen, whose stall torque is 74% of that of QDD.

| Motor | | | | | | |
|-------|---------|--------|------------------------|-----------|---------------|----------------|
| Power | Voltage | Mass | Inertia | Friction | ω_{nl} | τ_{stall} |
| [W] | [V] | [kg] | [kg · m ²] | [Nms/rad] | [rad/s] | [Nm] |
| 90 | 24 | 0.1151 | 1.35E-05 | 1.33E-05 | 654.5 | 0.92 |

Table 4.3: Chosen SEA Motor Specifications

In this paper, this motor will be used for further simulations as a chosen SEA motor. And, candidates of the rest of the SEA parameters can be shown in the table below.

| No. | Gearhead | | | | Spring |
|-----|----------|------------------------|-------|------------|-----------|
| | Mass | Inertia | Ratio | Efficiency | Stiffness |
| | [kg] | [kg · m ²] | [-] | [-] | [Nms/rad] |
| 1 | 0.36 | 9.10E-07 | 26 | 0.81 | 100 |
| 2 | 0.36 | 5.00E-07 | 36 | 0.81 | 190 |
| 3 | 0.46 | 1.50E-06 | 43 | 0.81 | 280 |
| 4 | 0.46 | 1.50E-06 | 53 | 0.81 | 370 |
| 5 | 0.46 | 1.50E-06 | 66 | 0.81 | 460 |
| 6 | 0.46 | 1.50E-06 | 74 | 0.81 | 550 |
| 7 | 0.46 | 9.40E-07 | 81 | 0.72 | 640 |
| 8 | 0.46 | 1.50E-06 | 91 | 0.72 | 730 |
| 9 | 0.46 | 9.40E-07 | 113 | 0.72 | 820 |
| 10 | 0.46 | 1.40E-06 | 126 | 0.72 | 910 |
| 11 | 0.46 | 9.10E-07 | 156 | 0.72 | 1000 |

Table 4.4: Candidates of SEA Gearbox and Spring

4.2.1 Trade-off Analysis

Roozing et al. 2017 [10] introduced two performance criteria for SEA as follows.

- **Transparency** : This shows how well the system can track the zero input torque with minimal residual torque produced by compliance. At low frequency, this can be improved by applying torque controller. However, at high frequency, stiffness of spring should be as low as possible to guarantee better performance.
- **Torque tracking** : This represents how well the system can track the input torque, when there is no output motion. For a better performance, higher stiffness is preferred.

In his research, selection guideline for optimal spring stiffness using pole placement and impedance rendering was mainly discussed, with no gear reduction. As Section 3.2 shows, non-unity gear reduction is also included in the control gain calculations, meaning that gear ratio has been included as an additional parameter.

4.2.2 Objective Function Formulation

The following objective function shows the costs which should be minimized.

$$E = \sum_{i=1}^4 W_i E_i = W_1 E_1 + W_2 E_2 + W_3 E_3 + W_4 E_4 \quad (4.2)$$

- **E_1) Torque tracking, $RMS(\tau_l^* - \tau_{l,s})$ (when $q_l = 0$)**
This means that there is a desired motion trajectory, whereas the arm does not rotate. Regardless of the zero motion, desired joint torque. τ_l^* is calculated due to the feedback for position controller. Torque controller should track this torque.
- **E_2) Transparency, $RMS(\tau_l^* - \tau_{l,s})$ (when $\tau_l^* = 0$)**
This means that the arm is not fixed, whereas τ_l^* is zero. This also means that desired trajectory is zero. Even though the torque input is absent, arm still moves due to the gravitational torque. In spite of the output error, torque controller should track this zero torque.
- **E_3) Friction Loss, $\int [n_s^2 (B_s + B_{g,s})] \dot{\theta}_s^2 dt$**
The idea is the same as QDD optimization. In this case, however, friction loss would be relatively dominant because of the large gear reduction.
- **E_4) Heat Loss, $\int \left(\frac{\tau_s}{K_{t,s}} \right)^2 R_{m,s} dt$**
The idea is the same as QDD optimization. However, heat loss would be minor due to the large gear reduction. [8]
- **W_i) Scaling factor, $\frac{w_i}{Min(E_i)}$**
As for normalization, the idea is the same as QDD optimization. In the case of weights, heat loss should be minor, and the rest should be equally prioritized. Thus, weights were selected as $w_i = [w_1, w_2, w_3, w_4] = [0.3, 0.3, 0.3, 0.1]$.

Conditions for simulations are as follows. The same trajectory, q_l^* was used.

- $E_1 = RMS(\tau_l^* - \tau_{l,s})$, and $W_1 = \frac{0.3}{Min(E_1)}$
- $E_2 = RMS(\tau_l^* - \tau_{l,s})$, and $W_2 = \frac{0.3}{Min(E_2)}$
- $E_3 = \int [n_s^2 (B_s + B_{g,s})] \dot{\theta}_s^2 dt$, and $W_3 = \frac{0.1}{Min(E_3)}$
- $E_4 = \int \left(\frac{\tau_s}{K_{t,s}} \right)^2 R_{m,s} dt$, and $W_4 = \frac{0.1}{Min(E_4)}$

1) Torque Tracking ($q_l = 0$), 2) Transparency ($\tau_l^* = 0$), 3) Friction and Heat Loss ($q_l, \tau_l^* \neq 0$)

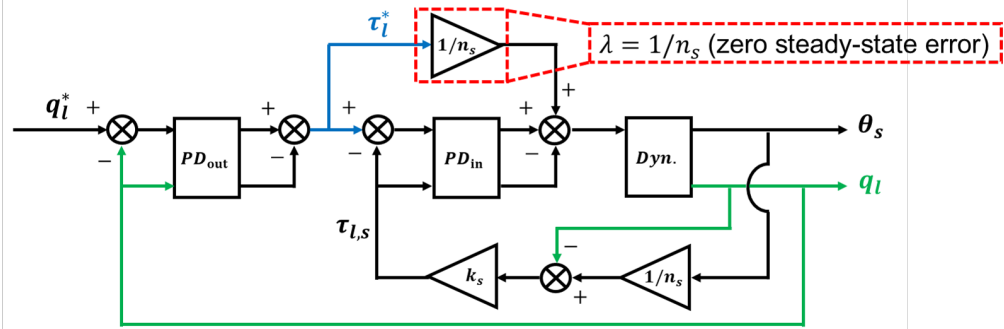


Figure 4.4: Test Scenarios for SEA Costs

4.2.3 Final Selection of Gearbox and Spring

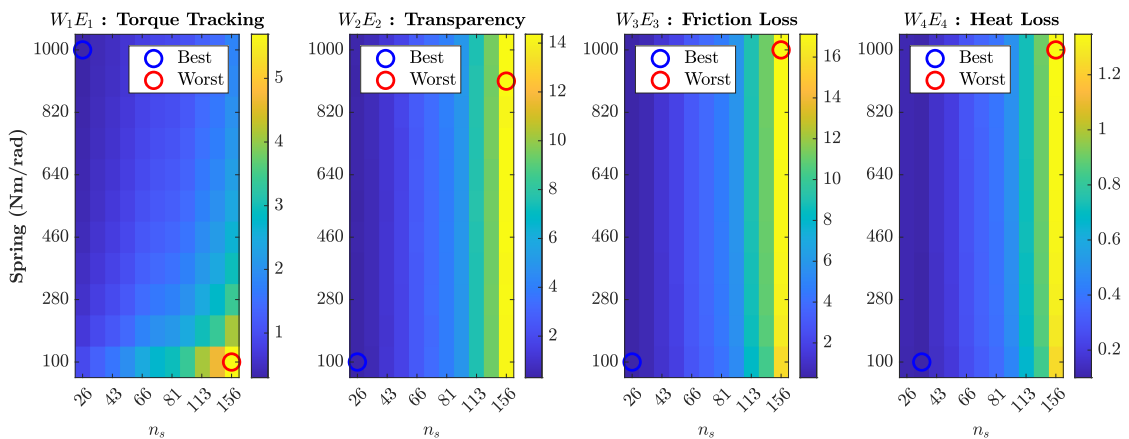


Figure 4.5: Colormaps of Scaled Costs of SEA Optimization

Figure 4.5 shows the colormaps plotted with the calculated costs. As for torque tracking, the trend was shown as the same as the observation. And W_1E_1 shows that torque tracking is dependent on both spring stiffness and gear ratio. However, the rest of the costs showed the opposite trends to W_1E_1 . Practically speaking, it can be seen that spring does not have a big influence on each performance, meaning that they are mainly related to gear reduction. As Figure 4.6 shows, since the best choice satisfied both speed and torque limits, the following gearbox and spring were chosen.

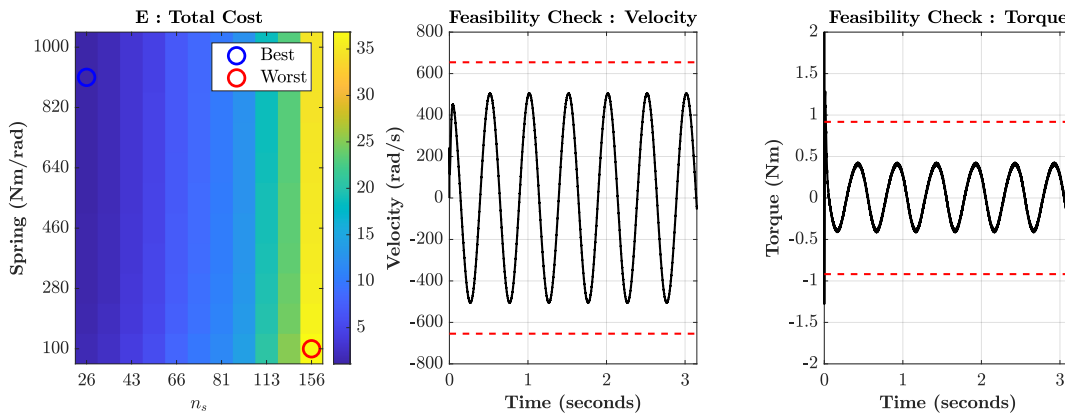


Figure 4.6: Feasibility Check of the Minimal Choice

| Gearhead | | | | Spring |
|----------|------------------------|-------|------------|-----------|
| Mass | Inertia | Ratio | Efficiency | Stiffness |
| [kg] | [kg · m ²] | [-] | [-] | [Nm/rad] |
| 0.36 | 9.10E-07 | 26 | 0.81 | 910 |

Table 4.5: Final Selection of SEA Gearbox and Spring

4.2.4 Gain Choice for Torque Control

Looking into the selected spring and gear ratio, it is seen that the current α can be lowered. As the right side of Figure 3.4 shows, even low value of α can make the controller sufficiently track the torque when high stiffness and low gear ratio are chosen. In this sense, gain tuning was done again with the chosen SEA parameters and the same set of α to make sure if gains can be lowered.

The right-hand side of Figure 4.7 shows the simulation result of torque tracking when α was set to 5.1. It is shown that the newly chosen α suffices for torque tracking.

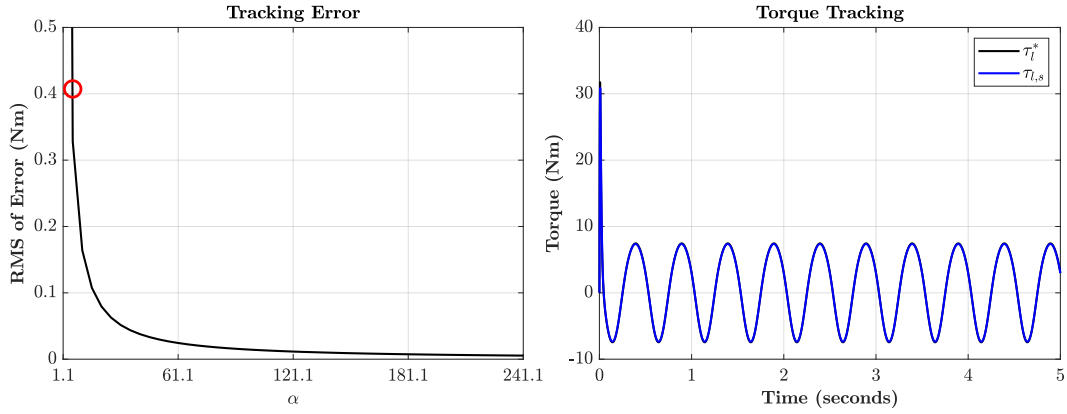


Figure 4.7: Test Results of Gain Tuning Simulations

Therefore, $\alpha = 5.1$ was chosen as a final value for closed-loop pole locations. Accordingly, control gains were calculated as $K_p = 0.96$, and $K_d = 0.0013$.

4.2.5 Final Selection

In the beginning, SEA motor was first chosen for simplification. In this subsection, results of SEA parameter optimization with multiple motor candidates will be shown. Table 4.6 shows a full list of SEA motor, gearbox and spring candidates.

| No. | Power [W] | Voltage [V] | Motor | | | | | Gearhead | | | | Spring Stiffness [Nm/rad] |
|-----|--------------|----------------|--------------|-----------------------------------|------------------------|--------------------------|------------------------|--------------|-----------------------------------|--------------|-------------------|---------------------------------|
| | | | Mass [kg] | Inertia [kg · m ²] | Friction [Nm·s/rad] | ω_{nl} [rad/s] | τ_{stall} [Nm] | Mass [kg] | Inertia [kg · m ²] | Ratio [-] | Efficiency [-] | |
| 1 | 60 | 18 | 0.1131 | 1.35E-05 | 1.36E-05 | 601.1 | 1.19 | 0.36 | 9.10E-07 | 26 | 0.81 | 100 |
| 2 | 60 | 24 | 0.1131 | 1.35E-05 | 1.31E-05 | 654.5 | 0.92 | 0.36 | 5.00E-07 | 36 | 0.81 | 190 |
| 3 | 60 | 36 | 0.1131 | 1.35E-05 | 1.33E-05 | 634.6 | 0.90 | 0.46 | 1.50E-06 | 43 | 0.81 | 280 |
| 4 | 60 | 48 | 0.1131 | 1.35E-05 | 1.36E-05 | 601.1 | 1.04 | 0.46 | 1.50E-06 | 53 | 0.81 | 370 |
| 5 | 90 | 18 | 0.1151 | 1.35E-05 | 1.38E-05 | 601.1 | 1.19 | 0.46 | 1.50E-06 | 66 | 0.81 | 460 |
| 6 | 90 | 24 | 0.1151 | 1.35E-05 | 1.33E-05 | 654.5 | 0.92 | 0.46 | 1.50E-06 | 74 | 0.81 | 550 |
| 7 | 90 | 36 | 0.1151 | 1.35E-05 | 1.35E-05 | 634.6 | 0.90 | 0.46 | 9.40E-07 | 81 | 0.72 | 640 |
| 8 | 90 | 48 | 0.1151 | 1.35E-05 | 1.37E-05 | 601.1 | 1.04 | 0.46 | 1.50E-06 | 91 | 0.72 | 730 |
| 9 | | | | | | | | 0.46 | 9.40E-07 | 113 | 0.72 | 820 |
| 10 | | | | | | | | 0.46 | 1.40E-06 | 126 | 0.72 | 910 |
| 11 | | | | | | | | 0.46 | 9.10E-07 | 156 | 0.72 | 1000 |

Table 4.6: Candidates of SEA Motors, Gearboxes and Springs

Through the process shown above, optimal combinations of gearbox and spring will be chosen per motor, and they will be compared. Figure 4.8 shows the colormaps for all the motor, gearbox and spring combinations. It can be seen that the minimal pair of spring and gearbox for all the cases is the same.

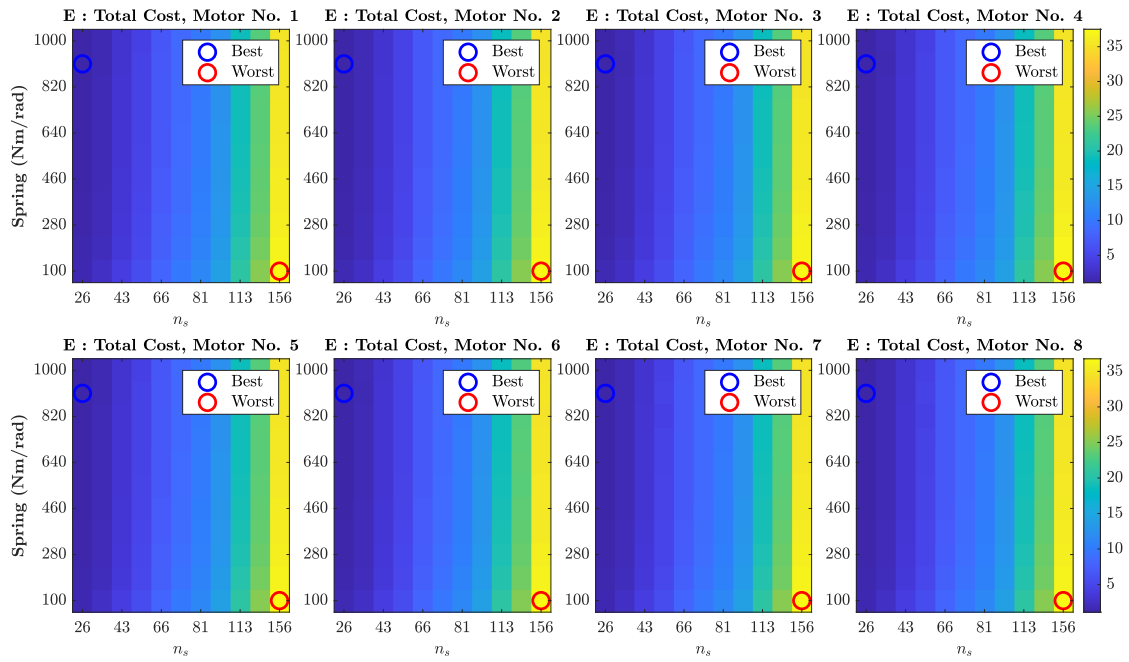


Figure 4.8: Colormaps of Total Costs of SEA Optimization, with Motors

Table 4.7 shows the calculated absolute costs (E_1 through E_4) and normalized total cost, E . As for torque tracking and transparency, all the motors show nearly the same performance. Considering the total cost, the 8th motor should be chosen as a final SEA motor, instead of the 6th one which is the same as the chosen one in the first place.

| No. | Motor | | | | | | | | Absolute Costs | | | | Total Cost E [-] |
|-----|--------------|----------------|--------------|-----------------------------------|------------------------|--------------------------|------------------------|---------------|----------------|--------------|--------------|---------|--------------------------|
| | Power [W] | Voltage [V] | Mass [kg] | Inertia [kg · m ²] | Friction [Nm·s/rad] | ω_{nl} [rad/s] | τ_{stall} [Nm] | E_1 [Nm] | E_2 [Nm] | E_3 [J] | E_4 [J] | | |
| 1 | 60 | 18 | 0.1131 | 1.35E-05 | 1.36E-05 | 601.1 | 1.19 | 0.39121 | 0.00021 | 214.701 | 202.439 | 1.07958 | |
| 2 | 60 | 24 | 0.1131 | 1.35E-05 | 1.31E-05 | 654.5 | 0.92 | 0.39121 | 0.00016 | 154.018 | 257.133 | 1.09574 | |
| 3 | 60 | 36 | 0.1131 | 1.35E-05 | 1.33E-05 | 634.6 | 0.90 | 0.39122 | 0.00016 | 154.930 | 255.797 | 1.09945 | |
| 4 | 60 | 48 | 0.1131 | 1.35E-05 | 1.36E-05 | 601.1 | 1.04 | 0.39121 | 0.00019 | 188.576 | 218.702 | 1.09085 | |
| 5 | 90 | 18 | 0.1151 | 1.35E-05 | 1.38E-05 | 601.1 | 1.19 | 0.39121 | 0.00021 | 214.701 | 202.439 | 1.07958 | |
| 6 | 90 | 24 | 0.1151 | 1.35E-05 | 1.33E-05 | 654.5 | 0.92 | 0.39121 | 0.00016 | 154.126 | 257.192 | 1.10166 | |
| 7 | 90 | 36 | 0.1151 | 1.35E-05 | 1.35E-05 | 634.6 | 0.90 | 0.39121 | 0.00017 | 155.047 | 255.363 | 1.12034 | |
| 8 | 90 | 48 | 0.1151 | 1.35E-05 | 1.37E-05 | 601.1 | 1.04 | 0.39121 | 0.00018 | 188.619 | 219.349 | 1.07538 | |

Table 4.7: Result of SEA Optimization, including Motors

Implementation : 1-DOF Robot Arm

5.1 Parameter Overview

| Category | Parameters | | DD | QDD | SEA |
|------------|---------------------|----------------------------|----------|----------|----------|
| Actuator | Motor | Mass [kg] | 0.99 | 0.15 | 0.12 |
| | | Inertia [$kg \cdot m^2$] | 5.05E-04 | 1.81E-05 | 1.35E-05 |
| | | Friction [Nms/rad] | 3.17E-04 | 1.91E-05 | 1.33E-05 |
| | | Torque Const. [Nm/A] | 0.29 | 0.04 | 0.04 |
| | | Resistance [Ω] | 1.28 | 0.57 | 0.94 |
| | | Stall Torque [Nm] | 13.30 | 1.69 | 0.92 |
| | | No-load Speed [rad/s] | 207.35 | 473.33 | 654.50 |
| | Gearbox | Mass [kg] | - | 0.26 | 0.36 |
| | | Inertia [$kg \cdot m^2$] | - | 4.90E-07 | 9.10E-07 |
| | | Friction [Nms/rad] | - | 2.88E-04 | 2.66E-04 |
| Ratio [-] | | - | 6 | 26 | |
| Spring | Stiff. [Nm/rad] | - | - | 910 | |
| Controller | Torque | K_p [-] | - | - | 0.92 |
| | | K_d [-] | - | - | 1.30E-03 |
| | Position | K_p [-] | - | 428.81 | - |
| | | K_d [-] | - | 7.25 | - |
| Robot | Link | Mass [kg] | - | 1 | - |
| | | Inertia [$kg \cdot m^2$] | - | 0.03 | - |

Table 5.1: Parameters for 1-DOF Simulations

The table above summarizes the selected parameters for simulations. Using the reference profile shown in Eq. 3.6, performances of all the actuators will be compared with the following criteria.

- **Position Tracking**

Firstly, tracking performances should be checked to see whether the designed actuators manage to follow the desired trajectory properly.

- **Joint Torque**

Secondly, the resultant joint torques for QDD and SEA will be compared with that of DD. Especially for SEA, the resultant torque is equal to the elastic torque produced by spring stiffness and difference between joint and motor motions.

- **Energy Loss**

Last but not least, power losses caused by Joule heating and friction will be compared. And, total energy losses during the given time will also be shown.

5.2 Test Results : Single Actuators

The following figure shows the results for position tracking and resultant joint torques for all the actuator designs.

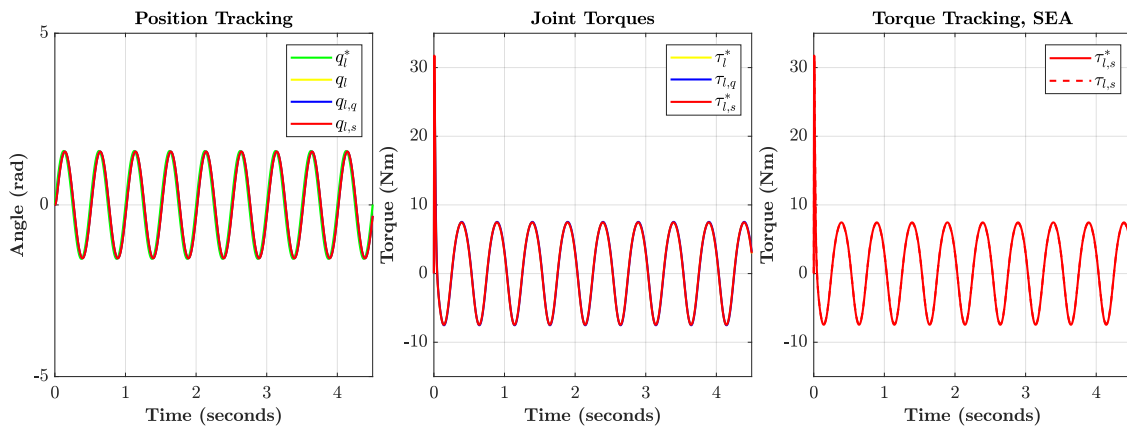


Figure 5.1: Position Tracking and Joint Torque

There is a minor phase difference between the desired and actual output motions of DD, which is seemed to be acceptable. As the left plot shows, tracking performances of QDD and SEA are nearly the same as DD. Also, shown in the middle figure, joint torques of QDD and SEA nearly matched that of DD, except for the instant peak. Especially for SEA, the instant peak shown is bigger than other two actuators. This is because SEA motor does not directly transfer torque to the link, but to the coupled compliance. Thus, bigger torque would be needed in the beginning. According to the right figure, SEA motor perfectly tracked the desired joint torque $\tau_{l,s}^*$.

Figure 5.2 shows the results of power losses. For an intuitive analysis, test data were filtered by a moving average filter with a 2Hz-sized window. As for QDD, heat loss is considerably dominant due to the low gear reduction. In the case of SEA,

heat loss is relatively low, compared to other two types. However, due to the higher gear ratio, friction loss much higher than DD or QDD.

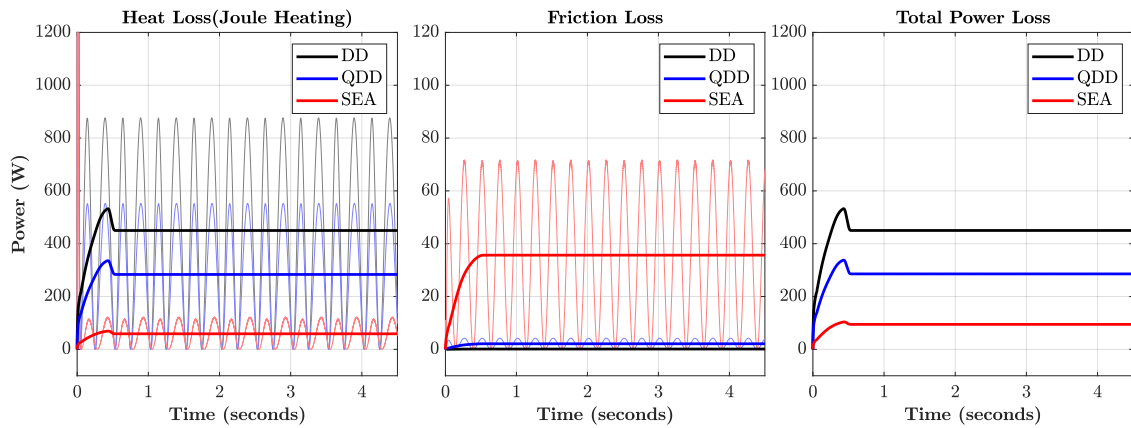


Figure 5.2: Power Loss of Actuators

Overall, total power loss of SEA is the lowest out of the three types. Table 5.2 summarizes the energy consumption over 4.5 seconds.

| Category | | DD | QDD | SEA |
|----------------------|-----|-------------|-------------------|------------------|
| Heat Loss | [J] | 2001 - - | 1261 (37.0%) ↓ | 261.25 (86.9%) ↓ |
| Friction Loss | [J] | 0.53 - - | 9.15 - - | 154.86 - - |
| Total Loss | [J] | 2001.53 - - | 1270.15 (36.5%) ↓ | 416.11 (79.2%) ↓ |

Table 5.2: Energy Consumption of Actuators

5.3 Redundant Actuation Design

Shown in the previous section, DD can be replaced with either QDD or SEA. Especially for energy consumption, SEA can play a role in saving the energy loss caused by motor heating. However, both of them are not always ideal as single actuators, due to the performance limits; torque capacity for QDD and torque bandwidth of SEA. Two scenarios can be a good example of this limitation issue. The first situation is that the bandwidth of the joint torque increased. Due to high gear reduction and compliance, SEA has a limited bandwidth for torque tracking, in spite of its own torque controller. In this sense, if the frequency for the desired torque is too high, SEA cannot track the torque. [8]. Second, it is assumed that an additional load is placed at the end-effector, and the robot should follow the same trajectory. If the QDD motor drive's maximum torque is not sufficient, this cannot be done.

A possible solution to tackle this issue is to apply double actuators onto the single joint. This paper will introduce the way to combine QDD and SEA to make such a redundant actuator design, so that the advantages of each concept can only be used; minimizing the energy consumption of QDD as well as compensating the limited torque tracking performance of SEA.

5.3.1 Torque Distribution

For a redundant actuator, an effective way to divide an input torque to QDD and SEA should be concerned. As Figure 5.3 shows, the idea is to distribute the low frequency torque to SEA and transfer the rest to QDD.

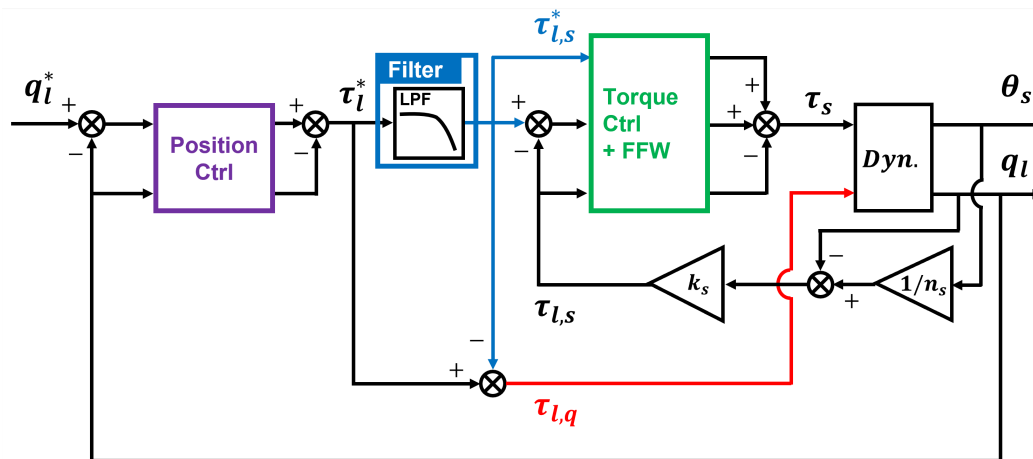


Figure 5.3: Block Diagram of Low Pass Filtering for Torque Distribution

Roozing et al. [8] introduced a concept of torque distribution using low pass filter. Malzahn et al. [16] introduced how to realize torque bandwidth using a chirp signal and a low pass filter. In this work, a heuristic method to realize torque bandwidth will be shown, on behalf of discrete time frequency response analysis. Torque tracking simulation shown in Section 4.2 can be done with SEA dynamics and a unit-sized chirp signal, which has frequencies ranging from 0.01 to 100Hz.

Figure 5.4 shows the test result with a duration of 100 seconds. This shows that SEA cannot track the input torque in the high frequency range. If the low frequency contents of the input can be realized, torque tracking performance can be guaranteed by transferring the low frequency torque to SEA and the high one to QDD. As a heuristic and intuitive way, error analysis can be done with a 1st order Butterworth filter and varying cutoff frequencies.

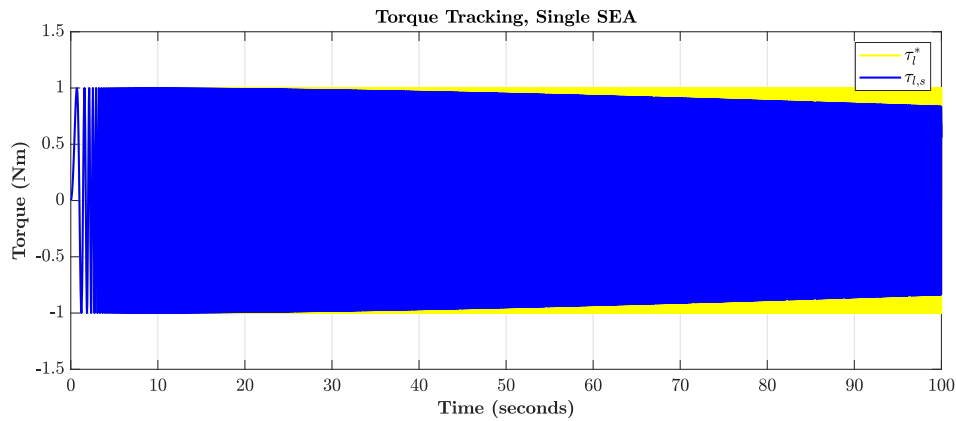


Figure 5.4: Torque Tracking of Single SEA, with a Chirp Signal

The left side of Figure 5.5 shows the RMS of the tracking error with varying cutoff frequency. From 5Hz, error level was lowered by about 3.5% of the amplitude of the input. The right figure shows that high frequency torque was transferred to QDD.

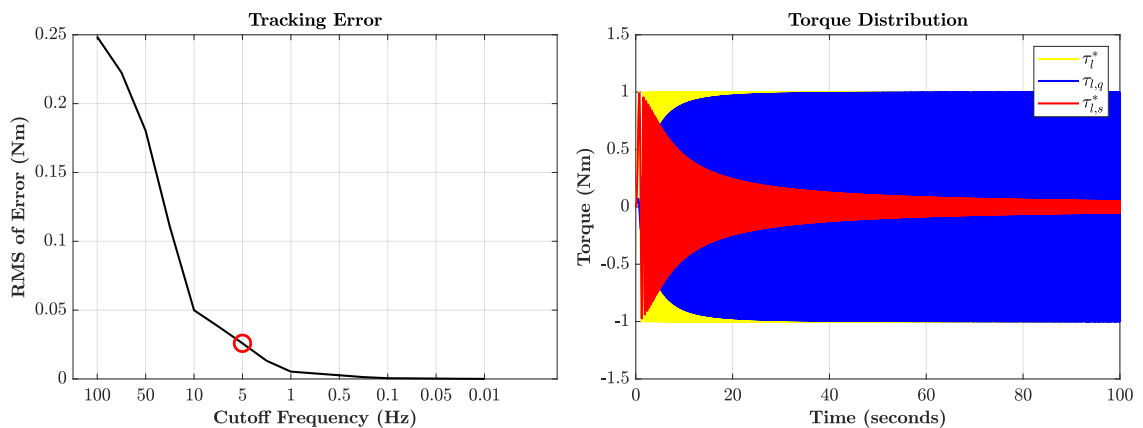


Figure 5.5: Torque Distribution, with 5Hz of Cutoff Frequency

In order to check if torque tracking was properly done, distributed and actual joint torques were compared in Figure 5.6. From the right-hand side of the figure showing the difference in magnitude and phase from $t = 50secs$, it is shown that the controller for SEA still has a limited tracking performance at high frequencies. In order to reduce the remaining tracking error, a proper cutoff frequency for this redundant actuator should be determined. In this case, error can be reduced by applying a lower cutoff frequency to the filter, so that QDD motor mainly tracks the joint torque more accurately. However, when it comes to the selection of cutoff frequency, it is noted that the torque capacity of both motors should also be taken into account. This will be discussed later.

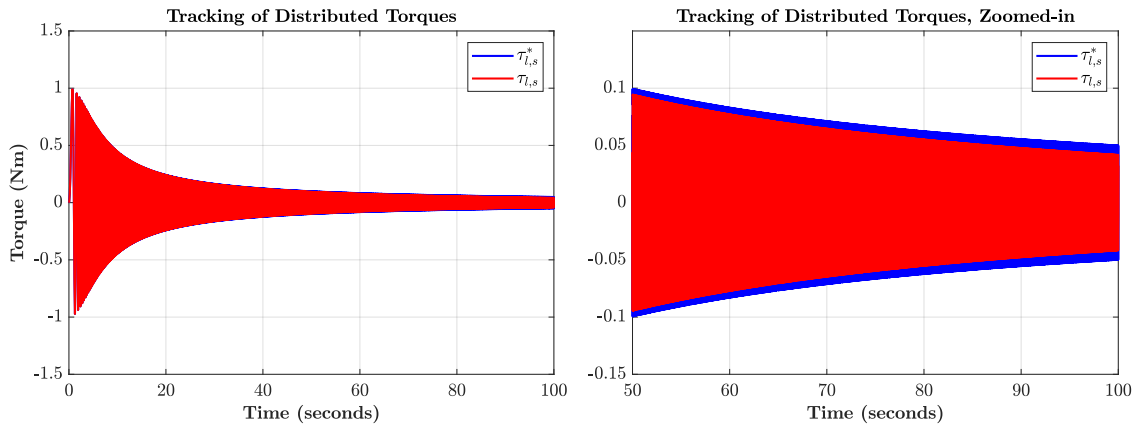


Figure 5.6: Distributed and Actual Joint Torques of SEA, with $\omega_c = 5Hz$

Figure 5.7 shows that an addition of QDD can be a solution to supplement limited torque bandwidth of single SEA. This can be a good solution for the increased bandwidth of joint torque, which is the first situation stated in the beginning.

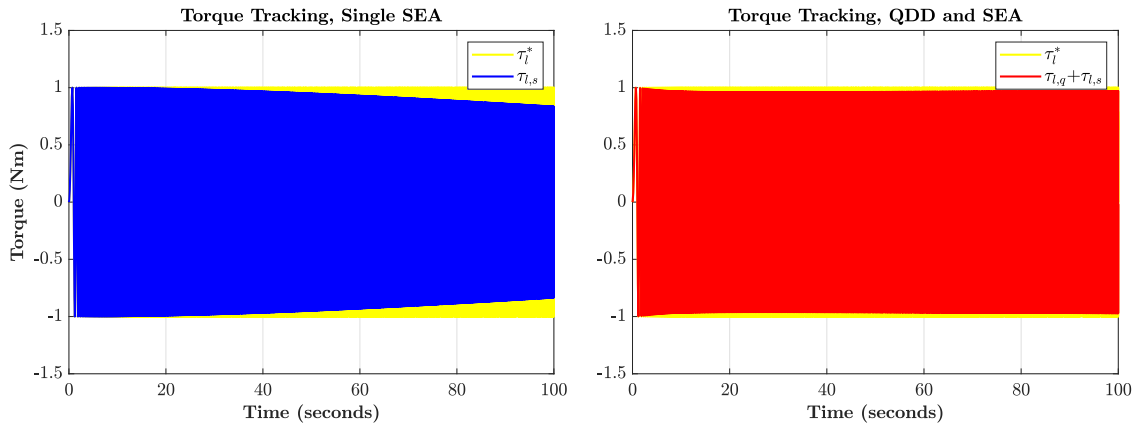


Figure 5.7: Position Tracking and Joint Torque, Redundant Actuator

Next simulation will show how the concept of torque distribution can resolve the torque capacity issue of QDD. An additional load weighing $3.5kg$ was added onto the end-effector. The following figures show the results of simulation with the same motion profile used in single actuator cases. From Figure 5.8, tracking performances and resultant joint torques for all the types were nearly at the same level. Figure 5.9 shows how the desired joint torque, $\tau_l^* = \tau_{l,q} + \tau_{l,s}^*$ is divided, and whether the actual elastic torque, $\tau_{l,s}$ tracks $\tau_{l,s}^*$ properly. According to the right side, actual SEA joint torque matches the filtered desired joint torque.

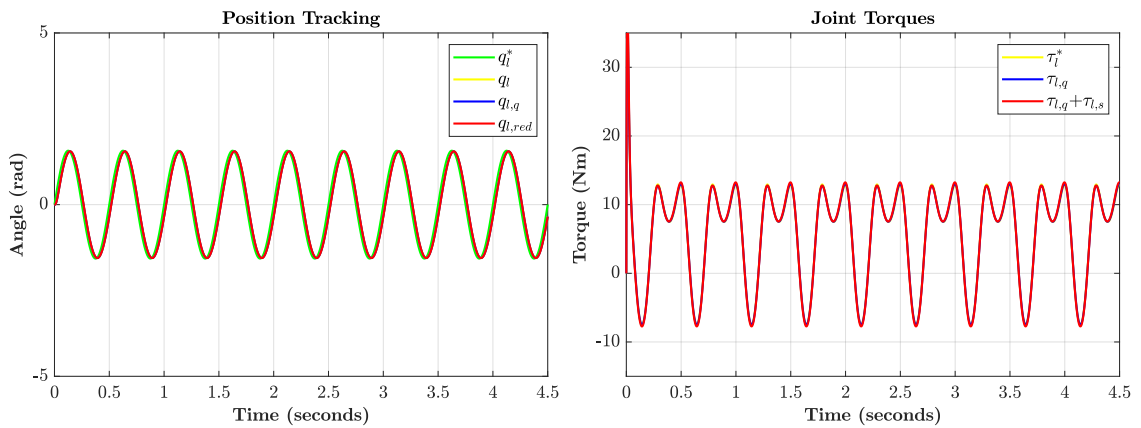


Figure 5.8: Position Tracking and Joint Torque, with an Additional Load

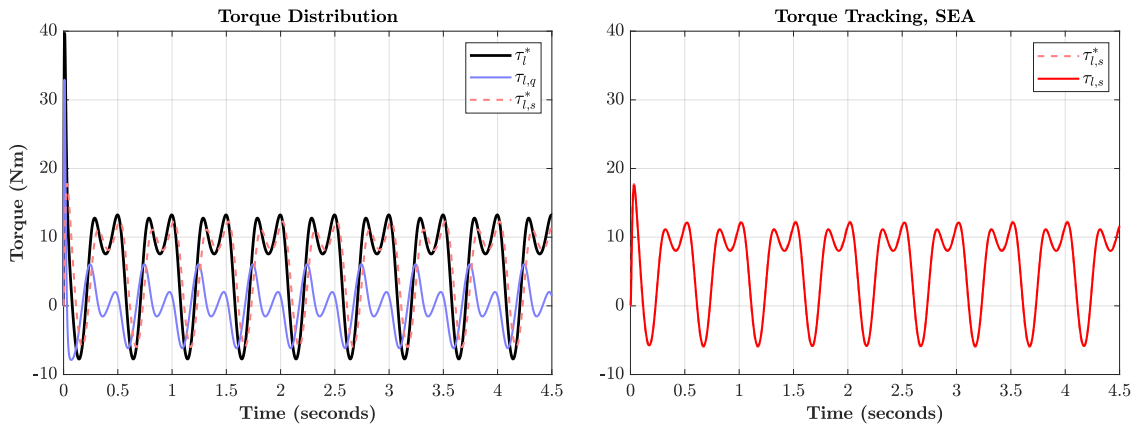


Figure 5.9: Torque Tracking Check of Redundant Actuator

Figure 5.10 shows the QDD motor torques before and after SEA was added. Shown in the left figure, it is not possible for a single QDD to be used for this scenario because the calculated motor torque is bigger than the maximum torque of QDD, which is its stall torque. By applying a redundant design, due to the supplementary torque produced by SEA, QDD motor torque was properly reduced. As Figure 5.11 shows, power consumption of a redundant actuator was less than 50% of that of a single QDD.

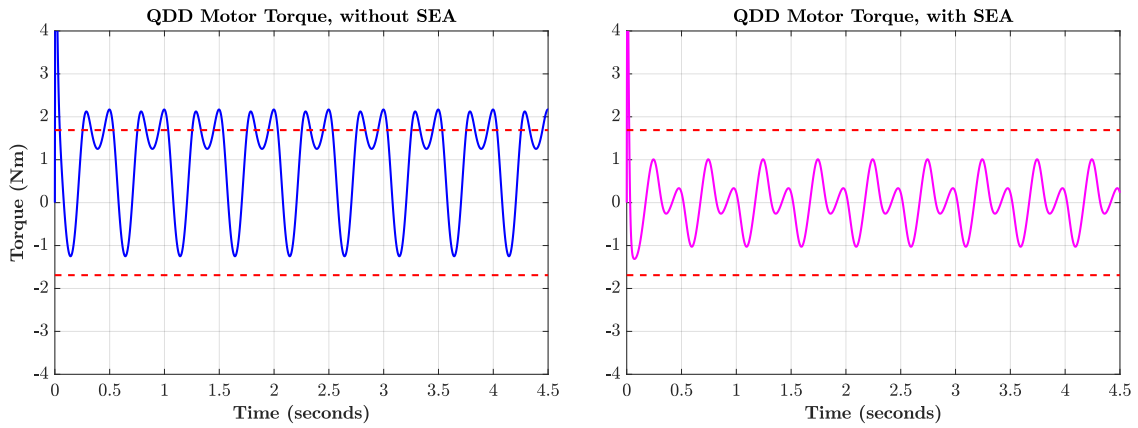


Figure 5.10: QDD Motor Torques, of Single and Redundant Actuators

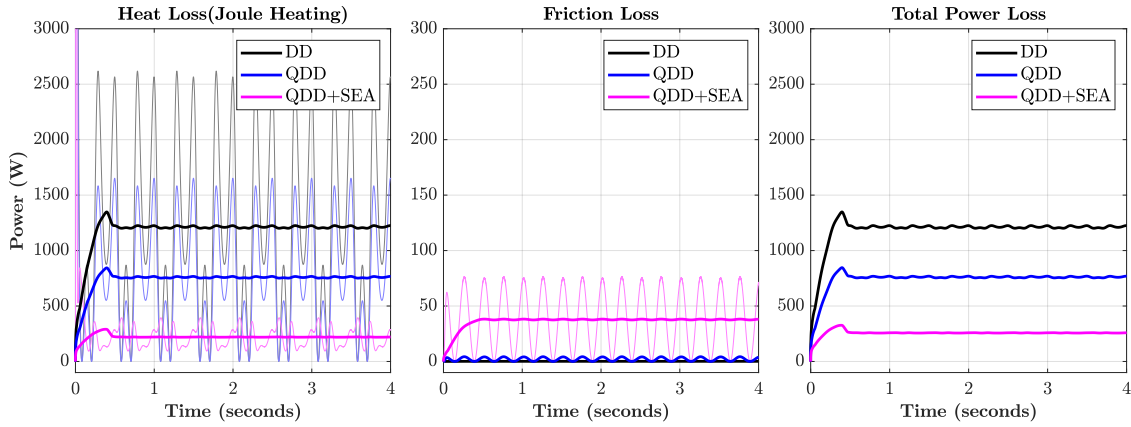


Figure 5.11: Power Loss of Actuators, with an Additional Load

5.3.2 Torque Tracking Performance

This subsection will show how the proposed actuator design can be evaluated. In order to check the torque tracking performance of the actuator, a torque profile will be tested with several conditions listed below.

$$\tau_l^* = A \sin 2\pi f t, \quad (5.1)$$

- **Cutoff Frequency, ω_c**

Six cutoff frequencies varying from 1 to 8 Hz were used. The purpose is to check the tracking performance with changing proportion of SEA elastic torque from the total joint torque.

- **Input Torque Profiles**

As for the frequencies(f) and amplitudes(A) of the input profiles, values ranging from $0.01Hz$ to $100Hz$ and those ranging from $1Nm$ to $35Nm$, which is nearly the sum of QDD and SEA maximum joint torques were used. The maximum for QDD equals the stall torque multiplied with gear ratio. Considering a static condition for SEA, it can be seen from Eq. 2.7 that the maximum for SEA can be obtained in the same way as QDD.

- **Saturation**

Saturation of motors should also be included to make the actuator not track the joint torque properly when each of the motor torques exceed the stall torques; $1.69Nm$ for QDD, and $0.918Nm$ for SEA, respectively.

Figure 5.12 shows the normalized tracking errors calculated with RMS of errors and amplitudes of the inputs. While the blue area indicates the tracking errors lower than 5%, yellow one shows the errors higher than 11% of the input magnitudes. And, it can be seen that the ratio of the two areas changes when cutoff frequency varies. As well as a performance assessment, this error analysis can also be a straightforward guideline to choose a proper cutoff frequency for the low-pass filter, so that an overall torque tracking performance of the redundant actuator with given inputs can be optimized.

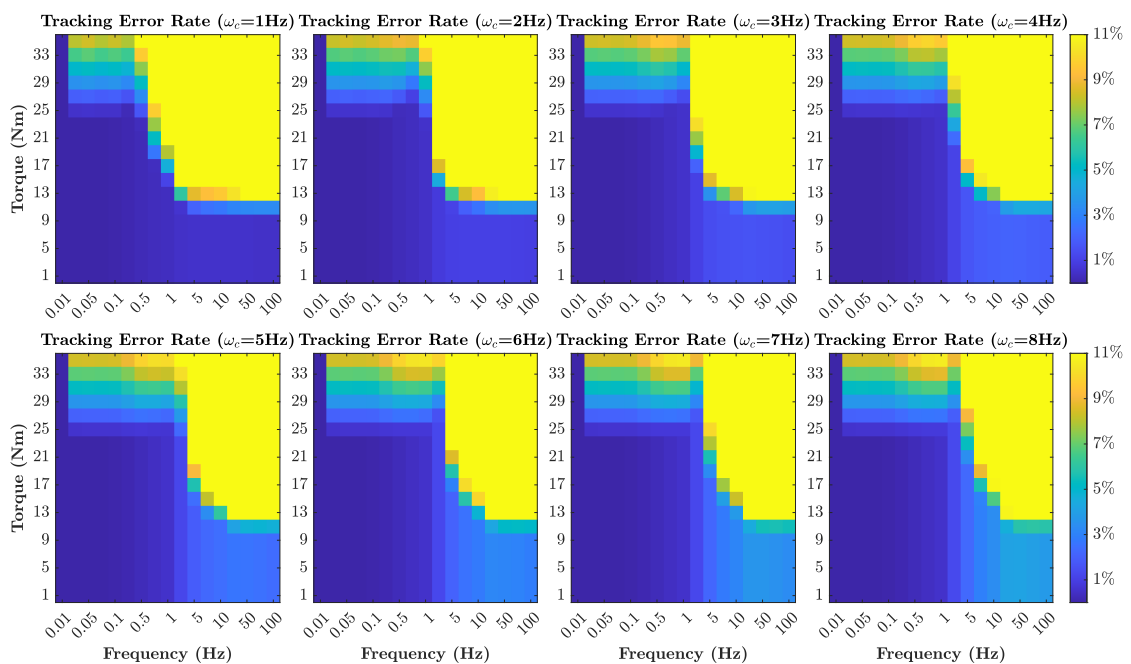


Figure 5.12: Torque Tracking Performance Check for Redundant Actuator

5.4 Test Results : Single and Redundant Actuators

The same simulation shown in Section 5.2 was done to compare single and redundant actuators. As Figure 5.13 shows, joint torques were distributed to QDD and SEA, and torque tracking of SEA was properly done. The results of energy consumption are shown in Figure 5.14 and Table 5.3.

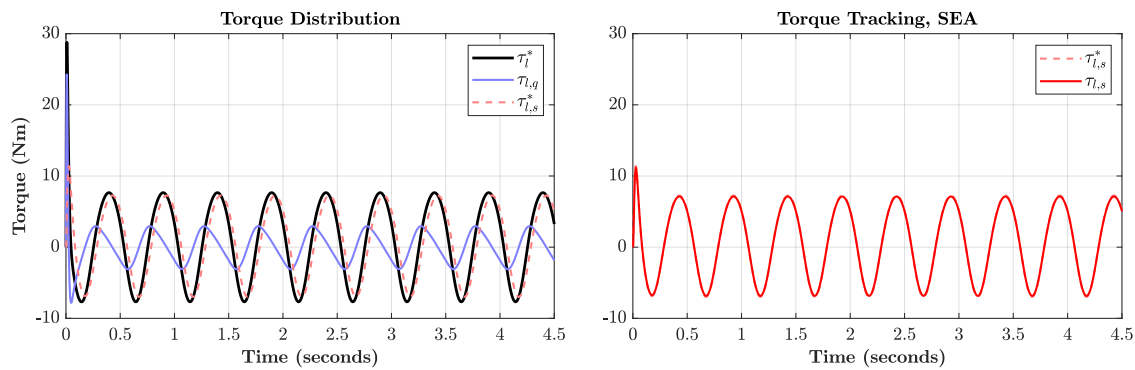


Figure 5.13: Torque Distribution and SEA Torque Tracking

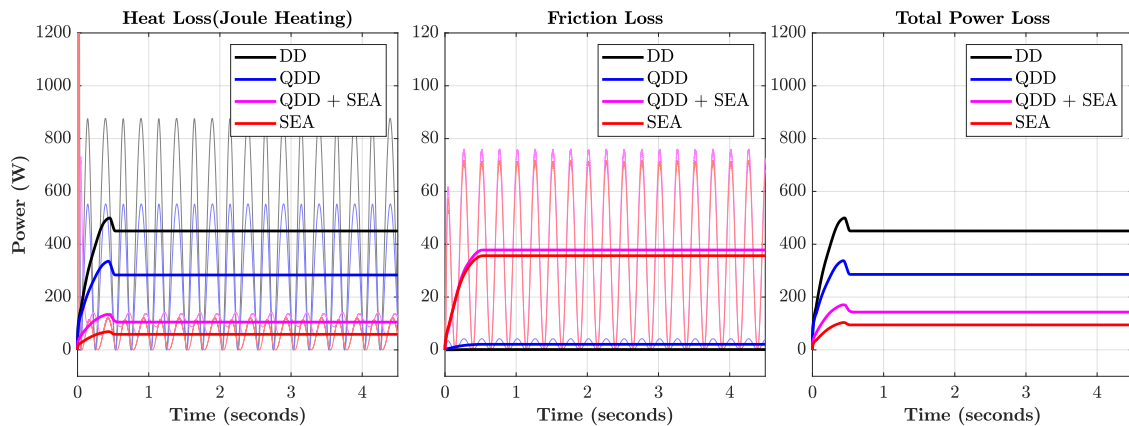


Figure 5.14: Power Loss of Single and Redundant Actuators

| Category | | DD | QDD | | QDD+SEA | | SEA | | | | | |
|---------------|-----|---------|-----|---------|---------|--------|--------|--------|-----|--------|-------|---|
| Heat Loss | [J] | 2001.00 | [-] | 1261.00 | 37.0% | ↓ | 472.52 | 76.4% | ↓ | 261.25 | 86.9% | ↓ |
| Friction Loss | [J] | 0.53 | [-] | 9.15 | [-] | 163.94 | [-] | 154.86 | [-] | | | |
| Total Loss | [J] | 2001.53 | [-] | 1270.15 | 36.5% | ↓ | 636.46 | 68.2% | ↓ | 416.11 | 79.2% | ↓ |

Table 5.3: Energy Loss of Single and Redundant Actuators, over 4.5 seconds

Implementation : 3-DOF Robot Leg

6.1 Position Control : Redundant Actuator

As stated at the end of Section 3.3, gain choice for the redundant actuator model will be shown. As for the cutoff frequencies of low pass filters for each SEA motor, they were chosen as $\omega_c = 1Hz$ as default. Considering the power consumption of the final simulations, they can be fine-tuned if it is needed. Figure 6.1 shows the error plots for the controllers.

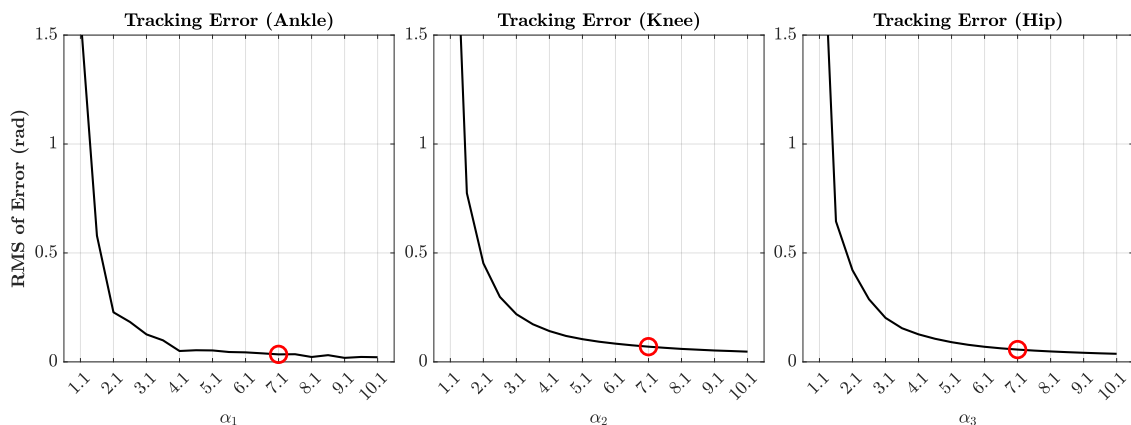


Figure 6.1: Test Results of Gain Tuning Simulations for Redundant Actuators

Errors for each of redundant joints show similar behaviors to those shown from DD gain tuning in Figure 3.6. This implies that control gains for redundant actuators would not have a big difference with those for DD actuators. With the same selection criteria shown previously, $\alpha = 7.1$ was chosen for all the joints.

6.2 Parameter Overview : Controller for 3-DOF Model

Except for the control gains for position controllers, all the parameters are the same as those used for 1-DOF simulations. As for this case, however, it is noted that the masses for actuators, except for that of ankle joint, were also included in the dynamics. Control gains of both position and torque controllers for final simulation are shown in Table 6.1.

| Category | Parameters | | DD | QDD | SEA |
|------------|------------|-------------------|---------|---------|----------|
| Controller | Torque | K_p [-] | - | - | 0.92 |
| | | K_d [-] | - | - | 1.30E-03 |
| | Position | $K_{p,ankle}$ [-] | 1085.40 | 1040.00 | |
| | | $K_{d,ankle}$ [-] | 61.59 | 60.28 | |
| | | $K_{p,knee}$ [-] | 499.13 | 419.37 | |
| | | $K_{d,knee}$ [-] | 24.11 | 22.115 | |
| | | $K_{p,hip}$ [-] | 44.67 | 72.71 | |
| | | $K_{d,hip}$ [-] | 3.13 | 3.96 | |

Table 6.1: Controller Settings for 3-DOF Robot Leg Simulations

As stated above, cutoff frequencies for each joint were started from 1Hz, and they can be changed considering power consumption level, which is mainly about motor heating. The motion profiles explained in Figure 3.5 were used for simulation, and the same criteria shown in Chapter 5 will be considered; position tracking, joint torques, and energy loss.

6.3 Test Results

Figure 6.2 shows the results of position tracking and resultant joint torque plots. The chosen cutoff frequency ($\omega_c = 1Hz$) for ankle and knee joints shows descent energy efficiency. In the case of hip joint, its torque profile is seemed to be relatively static compared to the others, meaning that a higher cutoff frequency can be applied to SEA motor to produce more torque because the frequency of the torque profile is lower than that of other two joint torques. In this sense, $\omega_c = 3Hz$ was chosen for the hip joint. And, It can be seen that both DD and redundant actuators properly follow the desired trajectories with a minor phase shift, similar to the 1-DOF simulations in Chapter 5. However, as for the joint torques for redundant actuators, instant peaks and oscillations were detected, and they became larger when the frequency of motion profiles increased. This happens when the end-effector changes the state of its motion, (from static to dynamic, or vice versa).

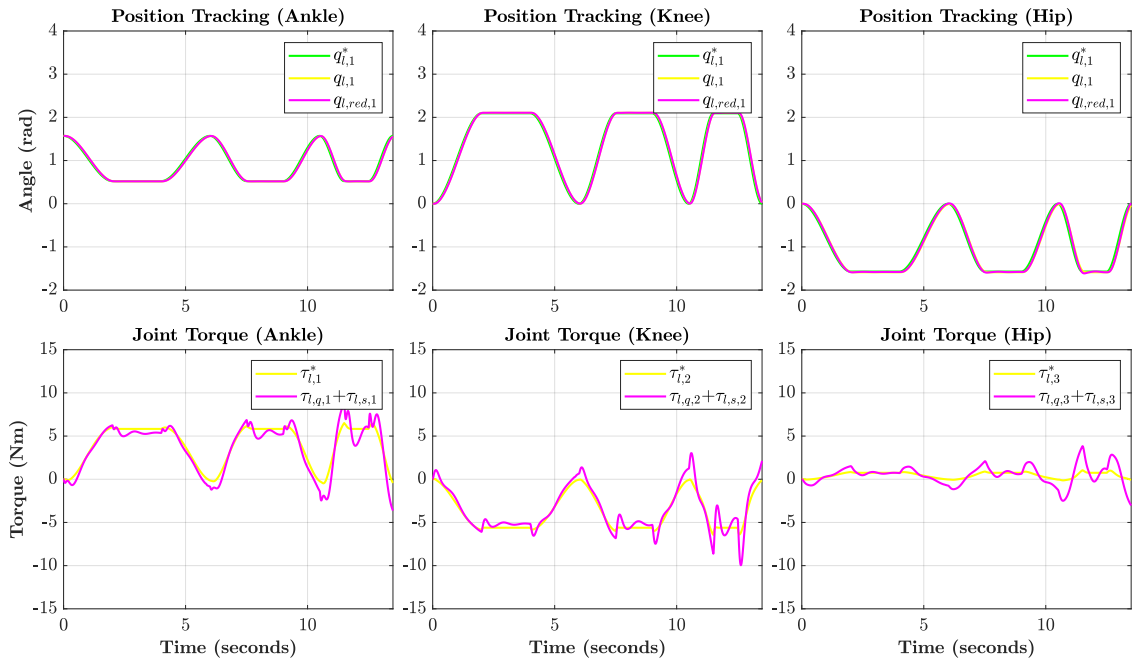


Figure 6.2: Position Tracking(Upper) and Joint Torques (Lower)

Figure 6.3 shows the curves for torque distribution and motor torques of QDD and SEA for each joint. From the plots on the second row, it is shown that SEA elastic torques, $\tau_{l,s}$ track the filtered joint torque, $\tau_{l,s}^*$ properly. Table 6.2 and Figure 6.4 show the energy consumption performances for the final simulations. Overall, redundant actuator shows quite a descent improvement in terms of energy efficiency, as well as similar position tracking performance compared to DD.

| Category | | | DD | | QDD+SEA | |
|-------------------|-------|-----|----------------|------------|---------------|----------------|
| Heat Loss | Ankle | [J] | 4509.41 | [-] | 444.62 | 90.1% ↓ |
| | Knee | [J] | 4041.67 | [-] | 405.02 | 90.0% ↓ |
| | Hip | [J] | 72.59 | [-] | 29.96 | 58.7% ↓ |
| Friction Loss | Ankle | [J] | 1.76.E-03 | [-] | 1.10 | [-] |
| | Knee | [J] | 7.06.E-03 | [-] | 4.45 | [-] |
| | Hip | [J] | 3.97.E-03 | [-] | 2.62 | [-] |
| Total Loss | | | 8623.68 | [-] | 887.76 | 89.7% ↓ |

Table 6.2: Energy Consumption of the Joints of 3-DOF Leg over 13.5 seconds

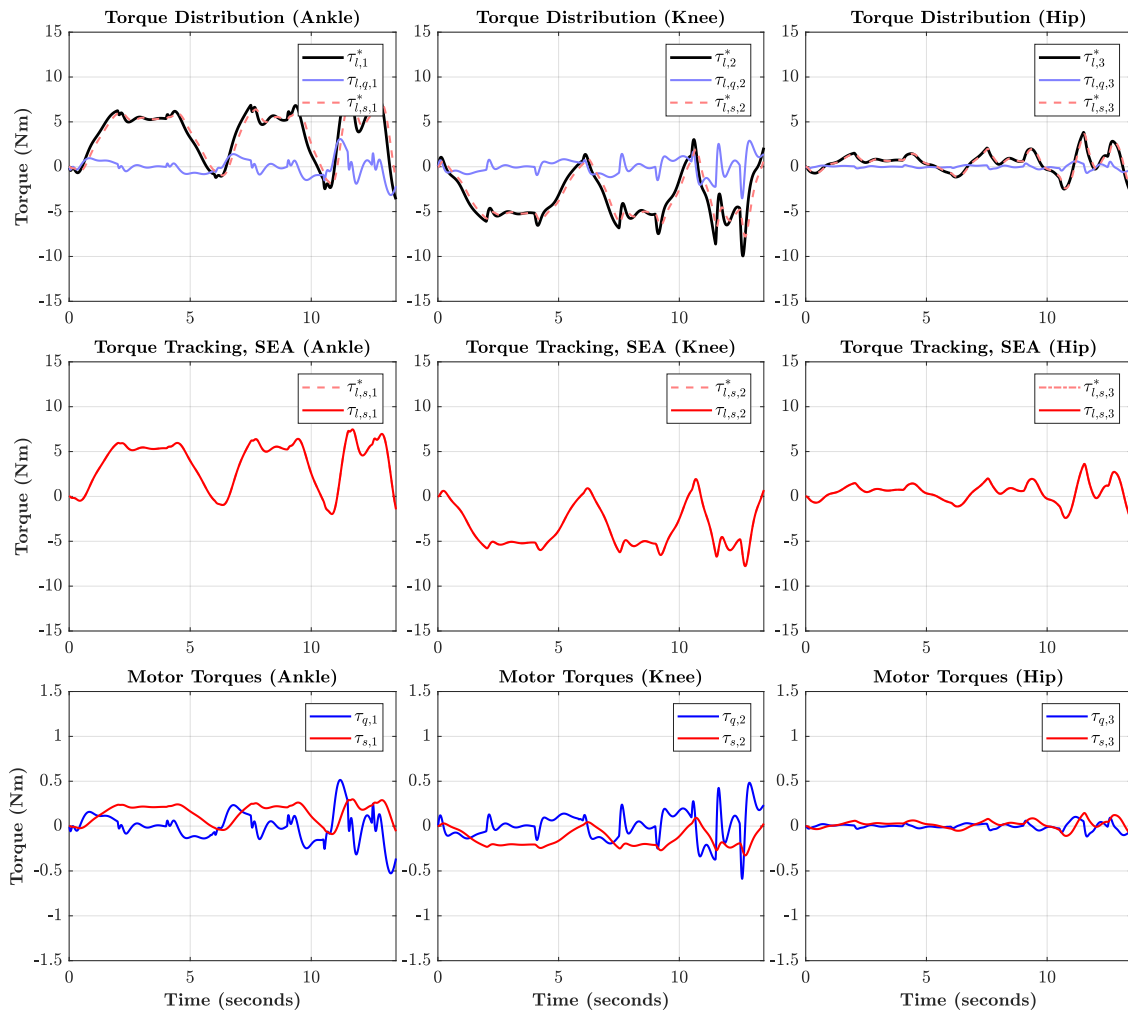


Figure 6.3: Torque Distribution (1st Row), SEA Torque Tracking (2nd Row) and Motor Torques (3rd Row) for Each Joints

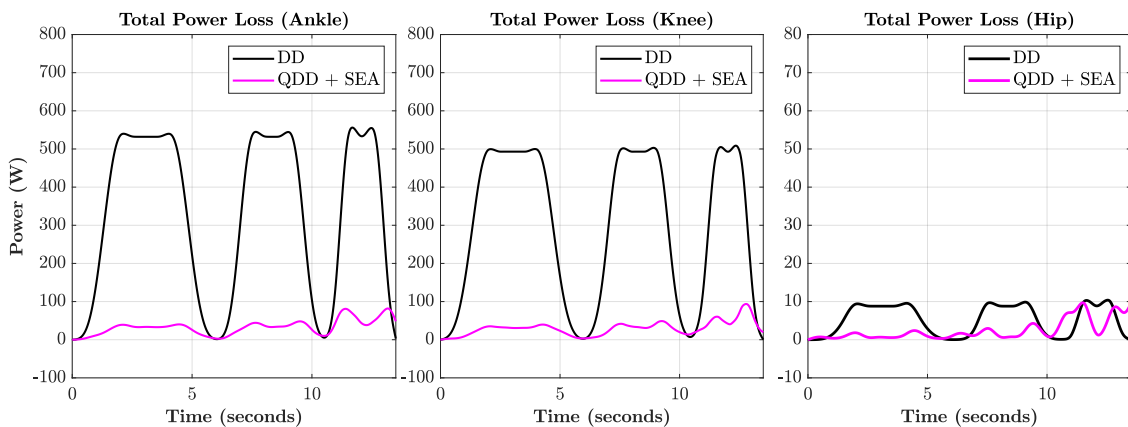


Figure 6.4: Power Loss of DD and Redundant Actuators

Conclusions and Future Work

7.1 Review of Research Questions

The listed research questions can be reviewed as follows.

- **What are the possible drawbacks that single actuators (QDD and SEA) cannot overcome?**

As for QDD, low gear reduction leads to significant energy loss caused by motor heating and lower torque capacity. In the case of SEA, compliance coupling makes it difficult to be controlled due to the lower control bandwidth. These intrinsic limitations of each type cannot be resolved when the system performance targets are too high in terms of speed and/or force(torque).

- **How to combine the concepts of both QDD and SEA to take advantage of the benefits and mitigate the disadvantages of each type?**

Two types of actuators can be made as one redundant actuator. By applying low-pass filtering, the desired force(torque) inputs can be divided into low-frequency and high-frequency contents, and transported to both SEA and QDD separately. This torque distribution enables to solve the two drawbacks stated above, as well as satisfying torque tracking performance and minimal motor power consumption, which are the benefits of QDD and SEA.

- **Which criteria are required for system parameter selection? How can the optimal system parameters be chosen in a mathematical way?**

When it comes to QDD, reflected inertia and power losses caused by friction and motor heating can be formulated as cost functions. In the case of SEA, mathematical formulation can be done for the two criteria related to torque control, torque tracking and transparency, as well as power losses. Using the scaling factors consisting of weights and minima for each cost, all the cost

values can become dimensionless indices. Parameters minimizing the total costs, which are the sums of all the scaled costs, can be chosen as optimal actuator parameters.

- **How to design actuation control systems for all the actuator dynamics which are nonlinear?**

There are two controllers required; one is a position controller for all the actuators, and the other is a torque controller, which improves control bandwidth of SEA. Using the linearized system dynamics and pole placement technique shown in Chapter 3, proper gains for optimal closed-loop performances in terms of both position and torque tracking can be determined.

- **How to evaluate the proposed design?**

Using the results of torque tracking performance check shown in Subsection 5.3.2, the redundant actuator can be assessed with different filter settings and input frequencies. This also implies that proper cutoff frequency can be chosen if the information of the input is known or can be estimated.

7.2 Final Remark

This paper shows how a powerful and energy-efficient actuator can be designed. The following items were mainly considered as the design targets; total weight and energy efficiency.

The first aim is to make the total weight of a redundant actuator lighter than or equal to that of DD actuator. In Table 5.1, it is shown that the design target in terms of total weight was already met. Secondly, test results of 1-DOF and 3-DOF simulations show that the redundant design has better energy efficiency, as well as similar tracking performance and resultant torques to those of DD. On top of that, in Subsection 5.3.2, it is shown that the proposed design, with similar weight and higher energy efficiency, can produce higher torques than DD actuator, having its limit at $13.3Nm$.

Considering all the observations stated, it leads to a conclusion that this work shows the possibility to design an actuator capable of producing higher forces(torques) as well as satisfying minimal energy consumption and similar physical dimensions. In conclusion, it can be said that the proposed actuator design can have two strong advantages; powerfulness and efficiency.

7.3 Future Work

Although the proposed design properly matches the topic of this work, there are still several tasks needed to be done as the parts of future work.

- **Individual Actuator Design**

Parameter optimization was done for a single pair of QDD and SEA, using a 1-DOF robot arm fixed at the world frame. This led to a less satisfactory performance shown from hip joint actuator in 3-DOF leg simulations. Since every joint would have different dynamic characteristics, a proper and promising method for an individual optimization of each actuator for multi-DOF system is required.

- **Controller and Low Pass Filter Design**

In this work, optimization was done for actuator parameters, only. Afterwards, gains for controllers and cutoff frequency for low-pass filter were selected through multiple trials of simulations, meaning that it would be time-consuming. If they can also be made into additional costs to be minimized and included into the optimization procedure, it would be more effective. As for control design, position and torque control schemes were only discussed. Thus, control design for physical interaction can also be done as the next step of this work.

- **Prototyping and Validation**

In this work, the possibility of designing the proposed actuator was shown through simulations, only. This means that there would be several external factors that are not taken into account; other types of frictions (Coulomb), disturbances and noises. Using the information of the selected robot parameters, a prototype can be made and tested in the real world, so that the unmodelled factors stated above can be included and the final performance of the proposed actuator design can be validated.

Bibliography

- [1] S. Seok, A. Wang, D. Otten, and S. Kim, "Actuator design for high force proprioceptive control in fast legged locomotion," in *2012 IEEE/RSJ International Conference on Intelligent Robots and Systems*, 2012, pp. 1970–1975.
- [2] S. Seok, A. Wang, M. Y. Chuah, D. J. Hyun, J. Lee, D. M. Otten, J. H. Lang, and S. Kim, "Design principles for energy-efficient legged locomotion and implementation on the mit cheetah robot," *IEEE/ASME Transactions on Mechatronics*, vol. 20, no. 3, pp. 1117–1129, 2015.
- [3] P. M. Wensing, A. Wang, S. Seok, D. Otten, J. Lang, and S. Kim, "Proprioceptive actuator design in the mit cheetah: Impact mitigation and high-bandwidth physical interaction for dynamic legged robots," *IEEE Transactions on Robotics*, vol. 33, no. 3, pp. 509–522, 2017.
- [4] S. Yu, T.-H. Huang, X. Yang, C. Jiao, J. Yang, Y. Chen, J. Yi, and H. Su, "Quasi-direct drive actuation for a lightweight hip exoskeleton with high backdrivability and high bandwidth," *IEEE/ASME Transactions on Mechatronics*, vol. 25, no. 4, pp. 1794–1802, 2020.
- [5] G. Pratt and M. Williamson, "Series elastic actuators," in *Proceedings 1995 IEEE/RSJ International Conference on Intelligent Robots and Systems. Human Robot Interaction and Cooperative Robots*, vol. 1, 1995, pp. 399–406 vol.1.
- [6] N. G. Tsagarakis, S. Morfey, H. Dallali, G. A. Medrano-Cerda, and D. G. Caldwell, "An asymmetric compliant antagonistic joint design for high performance mobility," in *2013 IEEE/RSJ International Conference on Intelligent Robots and Systems*, 2013, pp. 5512–5517.
- [7] N. G. Tsagarakis, H. Dallali, F. Negrello, W. Roosting, G. A. Medrano-Cerda, and D. G. Caldwell, "Compliant antagonistic joint tuning for gravitational load cancellation and improved efficient mobility," in *2014 IEEE-RAS International Conference on Humanoid Robots*, 2014, pp. 924–929.

- [8] W. Roozing, Z. Li, G. A. Medrano-Cerda, D. G. Caldwell, and N. G. Tsagarakis, "Development and control of a compliant asymmetric antagonistic actuator for energy efficient mobility," *IEEE/ASME Transactions on Mechatronics*, vol. 21, no. 2, pp. 1080–1091, 2016.
- [9] W. Roozing, Z. Ren, and N. Tsagarakis, "An efficient leg with series-parallel and biarticular compliant actuation: Design optimisation, modelling, and control of the eleg," *The International Journal of Robotics Research*, 12 2019.
- [10] W. Roozing, J. Malzahn, N. Kashiri, D. G. Caldwell, and N. G. Tsagarakis, "On the stiffness selection for torque-controlled series-elastic actuators," *IEEE Robotics and Automation Letters*, vol. 2, no. 4, pp. 2255–2262, 2017.
- [11] E. A. Bolívar Nieto, S. Rezazadeh, and R. D. Gregg, "Minimizing energy consumption and peak power of series elastic actuators: A convex optimization framework for elastic element design," *IEEE/ASME Transactions on Mechatronics*, vol. 24, no. 3, pp. 1334–1345, 2019.
- [12] G. Grandesso, G. Bravo-Palacios, P. M. Wensing, M. Fontana, and A. D. Prete, "Exploring the limits of a redundant actuation system through co-design," *IEEE Access*, vol. 9, pp. 56 802–56 811, 2021.
- [13] Maxon Group, "Maxon DC Motor and Maxon EC Motor, Key Information," 2014, https://www.maxongroup.com/medias/sys_master/8815460712478.pdf?attachment=true, Last accessed on 07-08-2022.
- [14] K. M. Lynch and F. C. Park, *Modern Robotics: Mechanics, Planning, and Control*, 1st ed. Cambridge University Press, 2017.
- [15] S. B. Niku, *Introduction to Robotics: Analysis, Control, Applications*, 2nd ed. Wiley, 2010.
- [16] J. Malzahn, N. Kashiri, W. Roozing, N. Tsagarakis, and D. Caldwell, "What is the torque bandwidth of this actuator?" in *2017 IEEE/RSJ International Conference on Intelligent Robots and Systems (IROS)*, 2017, pp. 4762–4768.

Mathematical Model for Leg Model

A.1 Equations of Motions : Direct-drive

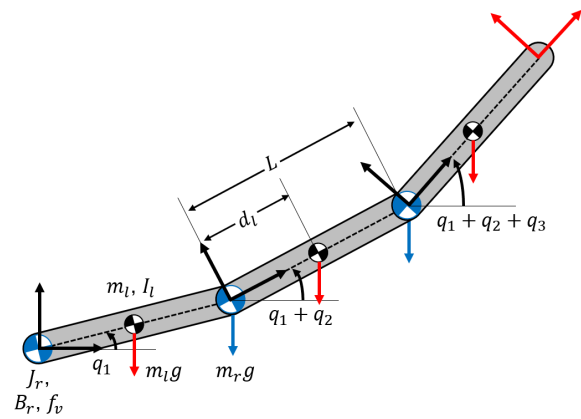


Figure A.1: 3-DOF Robot Leg with DD as Actuators

- **Symbolic Notations**

$q_1, q_2,$ and q_3 : Motor angles of Ankle, Knee and Hip Joints

$q_{ij} = q_i + q_j,$ and $q_{ijk} = q_i + q_j + q_k$

$I = I_l + J_r$ and $B = f_v + B_r$

- **Link 1 (Ankle Joint)**

$$K_1 = \frac{1}{2} I \dot{q}_1^2$$

$$P_1 = (m_l g d_l + m_r g L) \sin q_1$$

$$D_1 = \frac{1}{2} B \dot{q}_1^2$$

- **Link 2 (Knee Joint)**

$$x_2 = L\cos q_1 + d_l\cos q_{12}, \text{ and } y_2 = L\sin q_1 + d_l\sin q_{12}$$

$$v_2^2 = \dot{x}_2^2 + \dot{y}_2^2$$

$$K_2 = \frac{1}{2}I\dot{q}_{12}^2 + \frac{1}{2}m_l v_2^2$$

$$P_2 = m_l g(L\sin q_1 + d_l\sin q_{12}) + m_r g(L\sin q_1 + L\sin q_{12})$$

$$D_2 = \frac{1}{2}B\dot{q}_{12}^2$$

- **Link 3 (Hip Joint)**

$$x_3 = L\cos q_1 + L\cos q_{12} + d_l\cos q_{123}$$

$$y_3 = L\sin q_1 + L\sin q_{12} + d_l\sin q_{123}$$

$$v_3^2 = \dot{x}_3^2 + \dot{y}_3^2$$

$$K_3 = \frac{1}{2}I\dot{q}_{123}^2 + \frac{1}{2}m_l v_3^2$$

$$P_3 = m_l g[L\sin q_1 + L\sin q_{12} + d_l\sin q_{123}]$$

$$D_3 = \frac{1}{2}B\dot{q}_{123}^2$$

A.2 Equations of Motions : Redundant Actuator

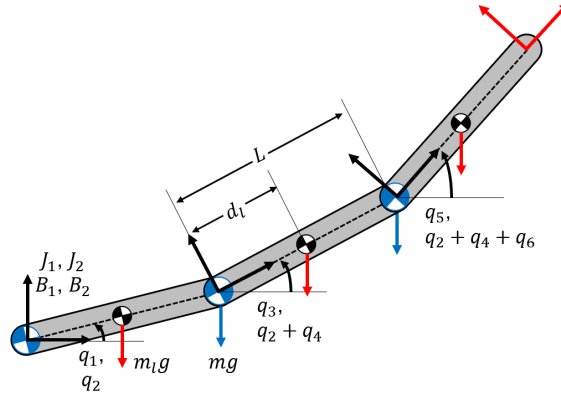


Figure A.2: 3-DOF Robot Leg with Redundant Actuators

• Symbolic Notations

$q_1, q_3,$ and q_5 : SEA Motor angles of Ankle, Knee and Hip Joints

$q_2, q_4,$ and q_6 : QDD Motor angles of Ankle, Knee and Hip Joints

$$J_1 = J_s + J_{g,s} \text{ and } J_2 = I_l + n_q^2(J_q + J_{g,q})$$

$$B_1 = B_s + B_{g,s} \text{ and } B_2 = f_v + n_q^2(B_q + J_{g,q})$$

$$m = m_s + m_{g,s} + m_q + m_{g,q}$$

• Link 1 (Ankle Joint), for SEA

$$K_1 = \frac{1}{2} J_1 \dot{q}_1^2$$

$$P_1 = \frac{1}{2} \frac{k_s}{n_s} \left(\frac{1}{n_s} q_1 - q_2 \right)^2$$

$$D_1 = \frac{1}{2} B_1 \dot{q}_1^2$$

• Link 1 (Ankle Joint), for QDD

$$K_2 = \frac{1}{2} J_2 \dot{q}_2^2$$

$$P_2 = m_1 g d_1 \sin q_2 + m g L \sin q_2 + \frac{1}{2} k_s \left(q_2 - \frac{1}{n_s} q_1 \right)^2$$

$$D_2 = \frac{1}{2} B_2 \dot{q}_2^2$$

- **Link 2 (Knee Joint), for SEA**

$$K_3 = \frac{1}{2} J_1 \dot{q}_3^2$$

$$P_3 = \frac{1}{2} \frac{k_s}{n_s} \left(\frac{1}{n_s} q_3 - q_4 \right)^2$$

$$D_3 = \frac{1}{2} B_1 \dot{q}_3^2$$

- **Link 2 (Knee Joint), for QDD**

$$K_4 = \frac{1}{2} J_2 \dot{q}_{24}^2$$

$$P_4 = m_l g (L \sin q_2 + d_l \sin q_{24}) + mg (L \sin q_2 + L \sin q_{24}) + \frac{1}{2} k_s \left(q_4 - \frac{1}{n_s} q_3 \right)^2$$

$$D_4 = \frac{1}{2} B_2 \dot{q}_{24}^2$$

- **Link 3 (Hip Joint), for SEA**

$$K_5 = \frac{1}{2} J_1 \dot{q}_5^2$$

$$P_5 = \frac{1}{2} \frac{k_s}{n_s} \left(\frac{1}{n_s} q_5 - q_6 \right)^2$$

$$D_5 = \frac{1}{2} B_1 \dot{q}_5^2$$

- **Link 3 (Hip Joint), for QDD**

$$K_6 = \frac{1}{2} J_2 \dot{q}_{246}^2$$

$$P_6 = m_l g (L \sin q_2 + L \sin q_{24} + d_l \sin q_{246}) + \frac{1}{2} k_s \left(q_6 - \frac{1}{n_s} q_5 \right)^2$$

$$D_6 = \frac{1}{2} B_2 \dot{q}_{246}^2$$